Journal of Molecular Liquids 275 (2019) 955–967

Contents lists available at ScienceDirect

Journal of Molecular Liquids

journal homepage: www.elsevier.com/locate/molliq

Adsorption behavior of metformin drug on boron nitride fullerenes: Thermodynamics and DFT studies

A.S. Ghasemi [a], Mohammad Ramezani Taghartapeh [b], Alireza Soltani [c,*], Peter J. Mahon [b]

[a] Department of Chemistry, Payame Noor University, P.O. Box, 19395-3697, Tehran, Iran
[b] Department of Chemistry and Biotechnology, Faculty of Science, Engineering and Technology, Swinburne University of Technology, Hawthorn, VIC 3122, Australia
[c] Golestan Rheumatology Research Center, Golestan University of Medical Science, Gorgan, Iran

ARTICLE INFO

Article history:
Received 2 August 2018
Received in revised form 21 November 2018
Accepted 23 November 2018
Available online 27 November 2018

Keywords:
Metformin
BN fullerenes
Adsorption
Density functional theory
Electronic structure

ABSTRACT

In this study, a density functional theory (DFT) calculation was carried out for the adsorption behavior and detection of metformin on the exterior surfaces of pure and doped boron nitride (BN) fullerenes by using B3LYP-D and PW91-D functionals. The results demonstrate that the —NH group of metformin can chemisorb on the boron atom of $B_{12}N_{12}$ and $B_{16}N_{16}$ fullerenes. Presence of polar solvent (water) increases the adsorption energy of metformin on the pure and $GaB_{11}N_{12}$ fullerenes. However, at the presence of Ga doping and it was found that the doping increases the binding energy of the metformin molecule, while the Ge doping decreases the binding energy. So our calculations suggest that the $GeB_{11}N_{12}$ has a greater sensitivity for the metformin molecule compared with the $GaB_{11}N_{12}$ fullerene. Our results represented that the $GeB_{11}N_{12}$ fullerene has good potential as a biosensor for the determination of metformin in environmental systems.

1. Introduction

Metformin ($C_4H_{11}N_5$) (MF) belongs to the biguanide family, which can play an effective role in the first-line pharmacological therapy of type 2 diabetes mellitus (T2DM) [1]. Nowadays, metformin is one of the most generally recommended drugs globally and has also been accepted for the treatment of hyperglycemia in England, Canada and the US. Moreover, metformin is a well-known drug in the treatment of type 2 diabetes mellitus with an established efficacy coupled with a favorable safety profile and low cost that has a diverse mechanism of action. Furthermore, it has been reported as an antiviral and anticancer enlivener [2]. Earlier studies have shown that metformin has immunomodulatory activity by influencing anti-inflammatory action on collagen-induced arthritis through the inhibition of IL-17-producing T (Th17) cells differentiation and the up-regulation of Treg cell differentiation along with the suppression of osteoclast differentiation [3]. On the other hand, nanoscience has revealed a unique and effective treatment behavior in medicine, specifically for the treatment of cancer cells and especially with the application of the promising nanomaterials such as boron nitride nanotubes in bone and soft tissue engineering [4–7].

Several analytical approaches have been used for the determination and sensing of the pure MF drug like high performance liquid chromatography (HPLC) [8–13], Gas Chromatography (GC) [14,15], conductometry [16], voltammetry [17–21], capillary electrophoresis [22], Mass spectroscopy [23], thermal and kinetic measurements [23], ultra-violet (UV–vis), infra-red (IR) and nuclear magnetic resonance (NMR) spectroscopies [24–33]. Moreover, they are some other approaches using ligands containing metal ions to form coordination complexes which facilitates its sensing and detection [23,34–39]. However, Computational DFT studies can prepare a condition to predict and cover many of these features like the bonding energies, optoelectronic and thermodynamic properties which are elaborated in the details in the present study to reduce the costs and time required for such studies.

Zhao et al. reported the use of magnesium, as a major electrolyte in human body indicating superior biocompatibility, in the stability from DNA nanoparticle as a new strategy with a non-toxic composition for tumor-targeted and pH responsive doxorubicin delivery [40]. Cai and co-workers have shown the effect of the magnesium oxide nanoparticles as an effective agricultural antibacterial agent against *Ralstonia solanacearum* in vitro and in vivo for the first time [41]. In a study, Suryavanshi and co-workers exhibited that the use of magnesium oxide nanoparticle (MgONP)-loaded electrospun polycaprolactone (PCL) polymer composites have potential as an efficient scaffold material for bone–soft tissue engineering applications [42].

Recently, studies on the small BN fullerenes have been extensively expanded both theoretically and experimentally owing to their isoelectronic analogy to fullerenes [43–47]. Theoretical reports have been presented for the fullerene-like $B_{12}N_{12}$ nano-clusters, where it has been realized that a cluster with an octahedron-like structure is made up of 4 hexagons and 6 squares are energetically the most stable configuration of clusters than the other mentioned counterparts [48] due to

* Corresponding author.
E-mail address: alireza.soltani@goums.ac.ir (A. Soltani).

https://doi.org/10.1016/j.molliq.2018.11.124
0167-7322/

their large energy gap [49–52]. Experimental characterization of the $B_{12}N_{12}$ clusters has been reported using high-resolution electron microscopy and laser desorption time-of-flight mass spectroscopy [53–55]. Moreover, nanoclusters generated from the atoms of groups III and V on the periodic table of elements are considered to be suitable replacements of pristine carbon nano-cages [56,57].

The adsorption behavior of various molecules or atoms on the $B_{12}N_{12}$ and $B_{16}N_{16}$ fullerenes has been previously investigated using DFT calculations [58–61]. Recently, a theoretical study on the interaction of adenine, uracil, and cytosine upon AlN and BN nano-cages was reported where the results indicated that the BN nano-cage is very sensitive to these amino acids compared with AlN nano-cage as a biochemical sensor [62]. Esrafili and Nurazar studied the adsorption and decomposition of methylamine (CH_3NH_2) on the surface of a $B_{12}N_{12}$ nano-cage [63]. Doping or decoration in BN nanostructures can dramatically change the structural and electronic properties, which can enhance their chemical sensing and bio-sensing behaviors [64–66]. Computational studies of Bahrami et al. showed that the $B_{12}N_{12}$ and Al-doped $B_{11}N_{12}$ nano-cages can be efficient adsorbents as well as used as a potential sensor for the detection of amphetamine in environmental systems [67]. Anota and Cocoletzi [68] reported the electronic and structural properties of metformin molecule on the surface and ends of (5, 5) BN nanotubes as being mostly chemisorption in nature. Recently, Javan et al. found that the 5-fluorouracil (keto-enol form) can covalently bond from its nitrogen head to the surface of a $B_{12}N_{12}$ nano-cage, whereas in the other forms from their study, it demonstrates only weak interactions owing to noncovalent bonds between the two species [69]. In a previous theoretical study, the adsorption of 5-aminolevulinic acid on the surfaces of $B_{12}N_{12}$ and $B_{16}N_{16}$ nanoclusters was considered using DFT calculations [70].

In this research, we aim to study the possibilities of BN fullerenes application in drug delivery technology. For this purpose, a series of systematic studies are performed on the covalent and non-covalent interactions of $B_{12}N_{12}$ and $B_{16}N_{16}$ fullerenes with MF followed by a complementary consideration of non-metal and metal-doped effects on the adsorption behavior and detection of this drug molecule. Interactions of MF with $CB_{11}N_{12}$, $GeB_{11}N_{12}$, $SiB_{11}N_{12}$, $GaB_{11}N_{12}$, $AlB_{11}N_{12}$ and $MgB_{11}N_{12}$ fullerenes have been studied and the nature of the chemical and physical interactions (noncovalent versus covalent) are reported.

2. Computational methods

Geometry optimizations, the density of states (DOS), frontier molecular orbital (FMO) and natural bond orbital (NBO) analyses were carried out with the Gaussian 09 quantum chemistry software package [71]. The adsorption of metformin on the pure $B_{12}N_{12}$ and $B_{16}N_{16}$ fullerenes were calculated and studied using DFT-D corrected Generalized Gradient Approximation/Perdew-Wang 91 (GGA/PW91, van der Waals interactions are considered with DFT-D correction) [72] and compared with Becke 3-parameter Lee-Yang-Parr augmented with an empirical dispersion term (B3LYP-D) [73–75] functional with the 6-311+G** standard basis set. The B3LYP and PW91 are indicated to be the dependable and usually applied methods in the study of different nanostructures [76–79]. The SCF convergence limit was set to 10^{-6} a.u. over energy and electron density. The thermodynamic parameters of the adsorption process consist of enthalpies (H), entropies (S) and Gibbs free energies (G). The IR vibrational frequencies for all models were computed in the gas phase with standard statistical thermodynamics at 298.14 K and 1 atm. In the (polarizable continuum model) PCM calculations, water was used as a solvent, with a value of $\varepsilon = 78.4$ for the dielectric constant. The adsorption energies (E_{ad}) of metformin upon the pristine BN fullerenes is calculated from

$$E_{ad} = E_{Fullerene-Molecule} - (E_{Fullerene} + E_{Molecule}) \quad (1)$$

where $E_{Fullerene}$ is the total energies of the pristine $B_{12}N_{12}$ and $B_{16}N_{16}$ fullerenes, respectively. $E_{Fullerene-Molecule}$ is the total energy of metformin interacting with the pristine $B_{12}N_{12}$ and $B_{16}N_{16}$ fullerenes. $E_{Molecule}$ represents the energy of an isolated metformin molecule.

3. Results and discussion

After optimization, the obtained B—N bond length in the 4 membered ring of $B_{12}N_{12}$ is 1.486 Å from Table 1 using the B3LYP functional and 1.492 Å from Table 2 using the PW91 functional. In addition, for the same bond in the 4 membered ring of $B_{16}N_{16}$ fullerene using B3LYP-D and PW91-D methods are 1.473 Å and 1.479 Å, respectively. Based on the B3LYP functional, the calculated energy band gap (E_g) between the highest occupied molecular orbital (HOMO) and lowest unoccupied molecular orbital (LUMO) for the $B_{12}N_{12}$ and $B_{16}N_{16}$ fullerenes were 6.84 and 6.37 eV, whereas in PW91-D method the E_g values for the $B_{12}N_{12}$ and $B_{16}N_{16}$ fullerenes 5.06 and 4.58 eV, respectively, which is in reasonable agreement with previous theoretical results [80,81]. The theoretical results demonstrate that the E_g value of $B_{12}N_{12}$ by PW91-D method is in good agreement with experimental results for $B_{12}N_{12}$ reported by the Oku et al. ($E_g = 5.1$ eV) [82]. Mulliken Population Analysis (MPA) charge values for N and B atoms of $B_{12}N_{12}$ with T_h symmetry were −0.441 and 0.441 electrons, while these values for the $B_{16}N_{16}$ fullerene with T_d symmetry were −0.450 and 0.450 electrons, respectively.

The reactivity of MF with $B_{12}N_{12}$ and $B_{16}N_{16}$ fullerenes has been studied in the various adsorption sites. The relaxed configurations for MF interacting with the $B_{12}N_{12}$ and $B_{16}N_{16}$ fullerenes are displayed in Fig. 1. In models **A** and **B**, the —NH group of the MF interacts with the fullerenes with models **C** and **D** showing the results when the —NH_2 group is interacting. The B3LYP calculations show that the MF molecule is a polar aromatic amino acid (5.23 Debye) and this will be useful in understanding how the polarity of an individual amino acid affects adsorption onto BN fullerenes [68]. Fig. 2 presents the optimized structures of the MF molecule adsorbed on the outer walls of the $B_{12}N_{12}$ and $B_{16}N_{16}$ fullerenes in vacuum phase. The chemisorption energies of MF molecule with the B atoms of $B_{12}N_{12}$ and $B_{16}N_{16}$ fullerenes in models **A** and **B** were calculated to be −1.36 and −1.32 eV with equilibrium distances of 1.58 and 1.59 Å (from —NH site of MF to the B atoms of $B_{12}N_{12}$ and $B_{16}N_{16}$ fullerenes) using the B3LYP-D functional, respectively. Anota and Cocoletzi have shown the chemisorption energy of −0.63 eV for metformin interacting with a BN nanotube [68], which is a weaker adsorption energy value compared to the findings in this present study. Hoseininezhad-Namin and coworkers also reported the interaction of metformin upon the SWCNT with weak binding energies of −0.07 eV (B3LYP) and −0.33 eV (ωB97XD) methods [83]. Therefore, the current results exhibit enhancements in the adsorption energies of MF upon B atoms of the studied BN fullerenes. These observations clearly show the influence of geometry, shape and generating atoms of an adsorbent on the physicochemical reactivity with MF molecule. The covalent interaction between MF and the $B_{12}N_{12}$ and $B_{16}N_{16}$ fullerenes leads to charge transfers of 0.26 and 0.28 electrons from MF to the fullerenes, respectively, indicating that the MF molecule acts as an electron donor and the fullerene acts as an electron acceptor.

The interaction between the MF molecule and the $B_{12}N_{12}$ and $B_{16}N_{16}$ fullerenes using PW91-D functional was also considered. It was clearly observed that MF molecule is closer to $B_{12}N_{12}$ and $B_{16}N_{16}$ fullerenes and revealed higher adsorption energies when it was computed with the PW91-D functional compared to those of computations with the B3LYP-D functional. The adsorption energies and interaction distance were −1.62 eV and 1.576 Å for the MF-$B_{12}N_{12}$ complex and −1.58 eV and 1.590 Å for the MF-$B_{16}N_{16}$ complex using the PW91-D functional calculation. The calculated length of $R_{N\text{-}H}$ ($R_{C\text{-}NH}$) bonds of the MF adsorbed on the $B_{12}N_{12}$ and $B_{16}N_{16}$ fullerenes are 1.014 (1.316) and 1.026 (1.308) Å by the B3LYP-D functional and 1.020 (1.325) and 1.019 (1.317) Å by the PW91-D functional, respectively, while these values for free drug molecule are 1.023 (1.282) Å by the B3LYP-D

Table 1
Calculated bond lengths (Å), bond angle (°), charges (Q/e), adsorption energy (E_{ad}/eV), distance (D/Å), HOMO energies (E_{HOMO}/eV), LUMO energies (E_{LUMO}/eV), HOMO-LUMO energy gap (E_g/eV), Fermi level energy (E_F/eV) and dipole moment (D_M/Debye) for the most stable configurations using the B3LYP-D functional.

System	MF	$B_{12}N_{12}$	$B_{16}N_{16}$	Model **A** NH-$B_{12}N_{12}$	Model **B** NH-$B_{16}N_{16}$	Model **C** NH_2-$B_{12}N_{12}$	Model **D** NH_2-$B_{16}N_{16}$
R_{B-N}	–	1.486	1.473	1.592	1.568	1.496	1.479
R_{B-N-B}	–	80.69	78.54	84.75	83.07	80.27	78.35
R_{N-B-N}	–	98.09	99.35	84.05	91.75	97.92	99.15
R_{N-H2}	1.015	–	–	1.018	1.013	1.016	1.015
R_{N-H}	1.023	–	–	1.014	1.026	1.011	1.021
R_{C-NH}	1.282	–	–	1.316	1.308	1.275	1.284
R_{C-NH2}	1.405	–	–	1.387	1.392	1.412	1.398
D/Å	–	–	–	1.570	1.594	2.346	2.294
E_{ad}/eV	–	–	–	−1.36	−1.32	−0.11	−0.10
Q_B	–	1.169	1.205	0.630	0.701	0.480	0.473
Q_N	–	−1.169	−1.205	−0.425	−0.517	−0.498	−0.495
Q_{NH2-MF}	−0.761	–	–	−0.409	−0.759	−0.795	−0.801
Q_{NH-MF}	−0.654	–	–	−0.413	−0.683	−0.581	−0.686
E_{HOMO}	−5.86	−7.71	−7.38	−6.32	−5.93	−5.96	−5.80
E_{LUMO}	0.72	−0.87	−1.01	−0.94	−0.91	−1.01	−1.23
E_g/eV	6.58	6.84	6.37	5.38	5.02	4.95	4.57
ΔE_g (%)	–	–	–	−21.35	−21.19	−27.63	−28.26
E_{FL}	−2.57	−4.29	−4.20	−3.63	−3.42	−3.49	−3.52
μ/eV	−2.57	−4.29	−4.20	−3.63	−3.42	−3.49	−3.52
η/eV	3.29	3.42	3.19	2.69	2.51	2.48	2.29
ω/eV	1.00	2.69	2.76	2.45	2.33	2.45	2.70
S/eV	0.15	0.15	0.16	0.19	0.20	0.20	0.22
χ/eV	2.57	4.29	4.20	3.63	3.42	3.49	3.52
D_M	5.23	0.0	0.0	11.327	15.380	4.486	5.637

functional and 1.023 (1.282) Å by the PW91-D functional (see Tables 1 and 2). This reveals that the PW91-D functional is closer to the results obtained from experimental data [84,85].

Supplementary studies were performed on the possible effects of a single dopant atom on the structural and electronic properties of the MF-$XB_{11}N_{12}$ complexes, where X is a B atom substituted by C, Mg, Al, Si, Ga or Ge atoms (Fig. 2). As a reference point, Table 3 contains the calculated results based on the B3LYP-D functional for all the doped $XB_{11}N_{12}$ fullerenes without the MF present. In comparison to the undoped fullerene listed in Table 1, the effect of substitution has increased the dipole moment, decreased the HOMO-LUMO gap, decreased Q_N and increased both R_{X-N} and R_{X-N-B} so that the replacement atom is displaced upwards from the cage. The obtained results reveal that the length of the C—N, Si—N, Mg—N, Al—N, Ge—N, and Ga—N bonds are increased to 1.487, 1.804, 2.072, 1.835, 1.918, and 1.905 Å, respectively, which is close to the calculated results by Bahrami [67] and Shakerzadeh [80]. As displayed in Table 4, the E_g value was reduced from 6.84 eV in free fullerene to 4.26 ($AlB_{11}N_{12}$), 5.77 ($SiB_{11}N_{12}$), 6.06 ($GeB_{11}N_{12}$), 4.55 ($CB_{11}N_{12}$), 4.32 ($MgB_{11}N_{12}$), and 3.76 eV ($GaB_{11}N_{12}$) after doping process, indicating remarkable changes in the electronic properties of doped $XB_{11}N_{12}$ fullerenes due to higher reactivity of doped systems than pure fullerene and can improve the sensing abilities of fullerene-based biosensors. This result is comparable with the obtained results by others [86–93].

Table 2
Calculated bond lengths (Å), bond angle (°), charges (Q/e), adsorption energy (E_{ad}/eV), distance (D/Å), HOMO energies (E_{HOMO}/eV), LUMO energies (E_{LUMO}/eV), HOMO-LUMO energy gap (E_g/eV), Fermi level energy (E_F/eV) and dipole moment (D_M/Debye) for the most stable configurations using the PW91-D functional.

System	MF	$B_{12}N_{12}$	$B_{16}N_{16}$	Model **A** NH-$B_{12}N_{12}$	Model **B** NH-$B_{16}N_{16}$
R_{B-N}	–	1.492	1.479	1.591	1.574
R_{B-N-B}	–	80.04	77.97	83.83	82.78
R_{N-B-N}	–	98.52	99.72	90.47	92.07
R_{N-H2}	1.022	–	–	1.020	1.019
R_{C-NH}	1.282	–	–	1.325	1.317
R_{C-NH2}	1.408	–	–	1.390	1.394
D/Å	–	–	–	1.567	1.590
E_{ad}/eV	–	–	–	−1.62	−1.58
Q_B	–	0.386	0.394	0.547	0.592
Q_N	–	−0.386	−0.394	−0.365	−0.451
Q_{NH2-MF}	−0.747	–	–	−0.390	−0.739
Q_{NH-MF}	−0.638	–	–	−0.395	−0.641
E_{HOMO}	−4.80	−6.82	−6.69	−5.44	−5.08
E_{LUMO}	−0.18	−1.76	−2.11	−1.82	−1.79
E_g/eV	4.62	5.06	4.58	3.62	3.29
ΔE_g (%)	–	–	–	28.46	28.17
E_{FL}	−2.49	−4.29	−4.40	−3.63	−3.44
μ/eV	−2.49	−4.29	−4.40	−3.63	−3.44
η/eV	2.31	2.53	2.29	1.81	1.65
ω/eV	1.34	3.64	4.23	3.64	3.59
S/eV	0.22	0.20	0.22	0.28	0.30
χ/eV	2.49	4.29	4.40	3.63	3.44
D_M	5.19	0.0	0.0	11.266	15.388

Table 5 represents the geometry and interaction energy values with the corresponding electronic property changes of the $XB_{11}N_{12}$ complexes. The calculations suggest that doping can have a profound positive effect on the adsorption process of the metformin molecule on the $XB_{11}N_{12}$ fullerenes [81,99,100]. The calculated E_{ads} values for the MF molecule interacting with the $CB_{11}N_{12}$, $GeB_{11}N_{12}$, $SiB_{11}N_{12}$, $MgB_{11}N_{12}$, $AlB_{11}N_{12}$, and $GaB_{11}N_{12}$ fullerenes are −0.62, −0.93, −1.26, −2.46, −2.72 and −2.78 eV using the B3LYP-D functional and the relative distances were computed to be 1.41, 1.80, 1.70, 2.15, 1.92 and 1.96 Å between the —NH group of the MF molecule and the X_{doped}-$B_{11}N_{12}$ fullerenes, respectively.

A comparison of the applied methods shows that the PW91-D functional produces insignificant differences in binding energy between the MF molecule and the doped-fullerenes relative to those computed with the B3LYP-D functional (Table 4). The results in the case of PW91-D functional calculations on the doped-$B_{11}N_{12}$/MT interaction systems generally reveal similar values compared to the same configurations calculated at the B3LYP-D functional (see Table 5). In the PW91-D functional, the values of E_{ads} for the MF molecule adsorbed over the $AlB_{11}N_{12}$ and the $GaB_{11}N_{12}$ fullerenes are calculated to be −2.80 and −2.85 eV, respectively (Table 5). Generally the adsorption values obtained at PW91-D functional for the interactions of the MT molecule with X_{doped}-$B_{11}N_{12}$ fullerenes are higher than those obtained by the B3LYP-D functional. Moreover, the energy gap values for the studied interaction configurations at PW91-D functional are lower than that of the B3LYP-D functional resulting to the possible higher conductivity of the adsorption systems and therefore higher charge transfers at the

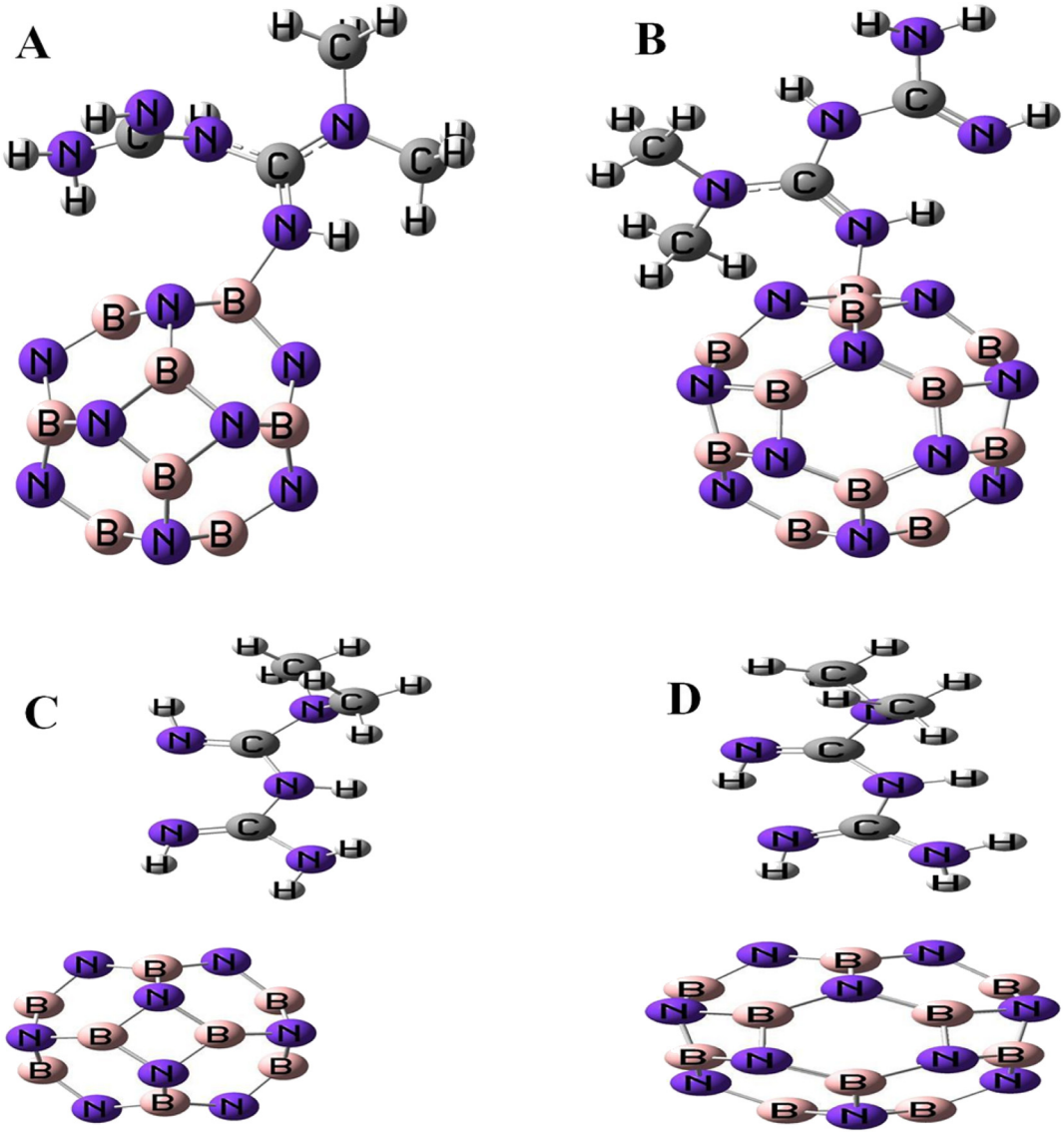

Fig. 1. Adsorption configurations of the MF molecule interacted with the pure $B_{12}N_{12}$ and the $B_{16}N_{16}$ fullerenes.

PW91-D functional (Table 5). Generally, for the same adsorption configuration, the energy gap difference value obtained by the PW91-D functional is more than that obtained by the B3LYP-D functional which results to the higher changes of the electronic properties of the entire system (Table 5). Moreover, the values for quantum molecular descriptor obtained using the PW91-D functional are comparably similar to those of the B3LYP-D while the dipole moment values of the same configurations are higher at PW91-D in comparison to the B3LYP-D (Table 5). Therefore, the above results indicate that the $GaB_{11}N_{12}$ fullerene interacting with the MF molecule will be more reactive at room temperature in comparison with the other doped-$XB_{11}N_{12}$ fullerenes using the B3LYP-D and the PW91-D functionals.

The highest E_{ads} (the most stable complex) is suggestive of a covalent interaction for the MF interacting with the $MgB_{11}N_{12}$, $AlB_{11}N_{12}$ and $GaB_{11}N_{12}$ fullerenes. Also, the MF molecule reacted with the Mg atom as a bidentate ligand through the two imine groups, which is similar to the experimental results reported by Soltani and co-workers [101]. In a recent study [48], the binding energies of −2.53 eV for the MF-Al-doped SWCNT using the ωB97XD functional and −1.33 eV for the MF-Si-doped SWCNT using the ωB97XD functional were reported. In a previous report, it has been shown that the binding energies of the 5FU (from its oxygen head) upon the Ge, Ga, and Al-doped BNNTs were shown to have values of −0.53, −1.50, and −1.86 eV; with interaction distances of 2.59, 2.01, and 1.88 Å between the MF molecule and the dopant atoms, respectively [102]. The current results show that the Al and Ga dopants can lead to improvement of the binding energy in the interaction between the MF molecule and the fullerenes and indicates a good agreement with all the above-mentioned results.

The present results indicate that the $B_{12}N_{12}$ fullerene has given better results for the interaction of the MF molecule compared to that of the $B_{16}N_{16}$ fullerene therefore the previous part has focused on the effect of doping on the $B_{12}N_{12}$ fullerene and using two DFT functional for more studies. Here, for a better understanding of the solvent effects on the adsorption systems and simulating the body condition, a set of PCM calculations was applied using water as the solvent for the studied adsorption configurations with the results summarized in Table 6. These were eventually compared with the calculations performed in the vacuum phase for the same adsorption configurations. The difference between these solvation energies is equal to E_{sol}. The solvation energies were calculated with the aid of the 'Conductor-like Screening Model' for solvation [94]. A considerable enhancement has been observed in the solvation energies of pure $B_{12}N_{12}$ and $GaB_{11}N_{12}$ after MF adsorption as

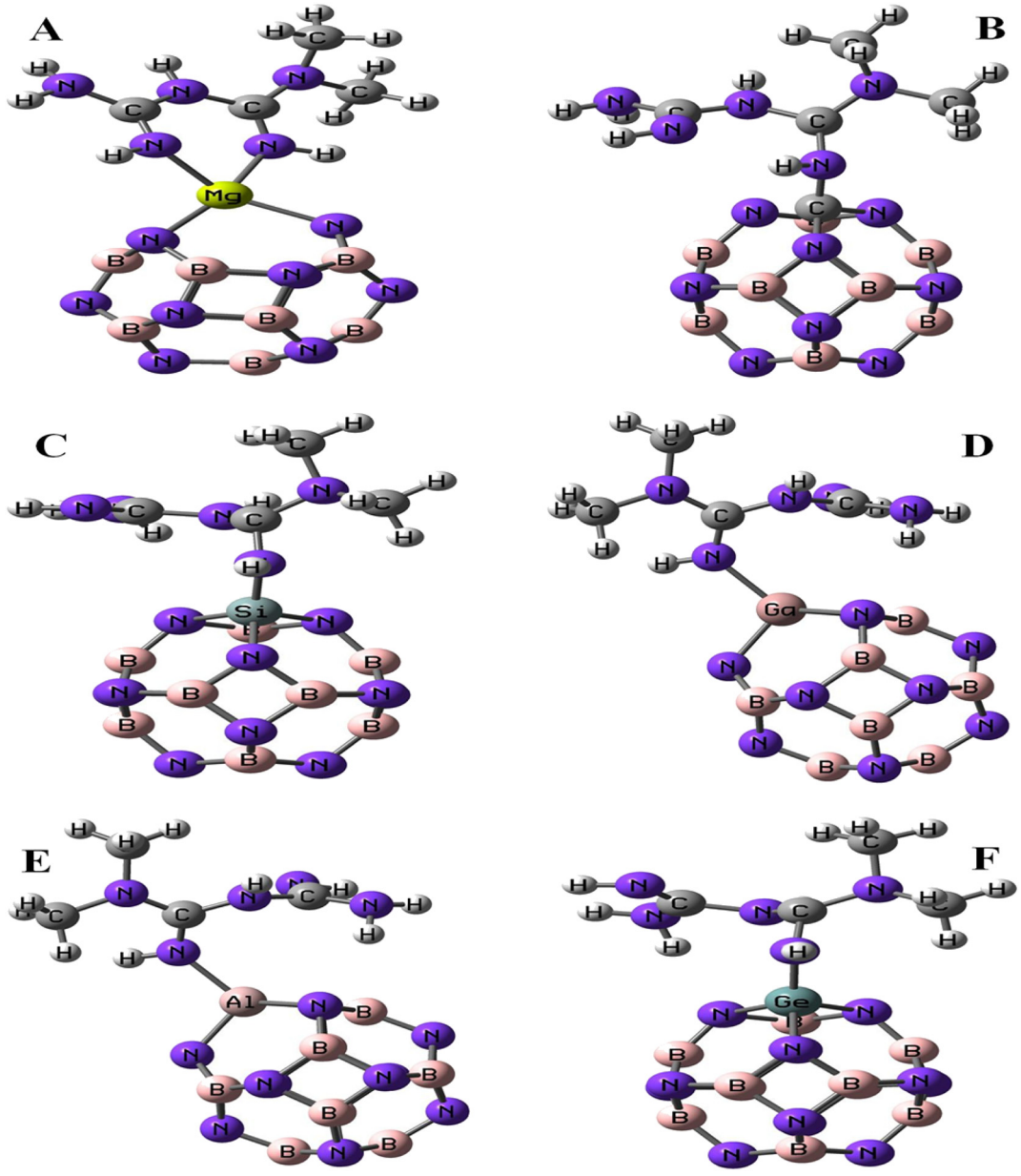

Fig. 2. Adsorption configurations of the MF molecule interacted with the non-metal and metal-doped $B_{12}N_{12}$ fullerenes.

Table 3
Calculated bond lengths (Å), bond angle (°), charges (Q/e), adsorption energy (E_{ad}/eV), distance (D/Å), HOMO energies (E_{HOMO}/eV), LUMO energies (E_{LUMO}/eV), HOMO-LUMO energy gap (E_g/eV), Fermi level energy (E_F/eV) and dipole moment (D_M/Debye) for the most stable configurations using the B3LYP-D functional.

System	$AlB_{11}N_{12}$	$SiB_{11}N_{12}$	$GeB_{11}N_{12}$	$CB_{11}N_{12}$	$MgB_{11}N_{12}$	$GaB_{11}N_{12}$
$R_{X\text{-}N}$	1.835	1.804	1.918	1.487	2.072	1.905
$R_{X\text{-}N\text{-}B}$	83.56	86.45	87.45	85.43	92.02	84.96
Q_X	0.613	0.752	0.572	0.314	0.615	0.497
Q_B	0.546	0.473	0.565	0.487	0.566	0.622
Q_N	−0.548	−0.557	−0.553	−0.433	−0.542	−0.600
E_{HOMO}	−7.31	−6.66	−7.03	−5.51	−6.83	−7.34
E_{LUMO}	−3.05	−0.89	−0.97	−0.96	−2.51	−3.58
E_g/eV	4.26	5.77	6.06	4.55	4.32	3.76
E_{FL}	−5.18	−3.78	−4.00	−3.24	−4.67	−5.46
μ/eV	−5.18	−3.78	−4.00	−3.23	−4.67	−5.46
η/eV	2.13	2.89	3.03	2.28	2.16	1.88
ω/eV	6.29	2.47	2.64	2.30	5.05	7.93
S/eV	0.23	0.17	0.16	0.22	0.23	0.26
χ/eV	5.18	3.78	4.00	3.23	4.67	5.46
D_M	3.237	0.947	1.548	0.692	5.415	2.763

summarized in Table 3. In contrast, E_{sol} for $GaB_{11}N_{12}$ is more energetic than that of pure $B_{12}N_{12}$ in both functionals. So, Ga doping on $B_{12}N_{12}$ fullerene improves the solvation energy [95]. This demonstrates that the increase in the solubility of the drug in the presence of fullerene in an aqueous system will enhance their suitability as carriers to deliver MF [68]. After structural relaxation, it was noticed that there was some structural deformations due to the transformation of sp^2 to sp^3 hybridization of the B atom on the exterior surfaces of $B_{12}N_{12}$ and $B_{16}N_{16}$ fullerenes, indicating that the adsorption process is exothermic. The physisorption energies in models **C** and **D** were −0.11 and −0.10 eV with equilibrium distances of 2.35 and 2.32 Å, respectively. In addition, these calculations demonstrate that the adsorption of the drug molecule leads to an overriding increase in the values of polarity compared to the pure fullerenes, with D_M = 11.33 and 15.38 Debye in models **A** and **B** computed by B3LYP-D functional, respectively. The results reveal that the major differences in the adsorption process between the MF molecule and $B_{12}N_{12}$ and $B_{16}N_{16}$ fullerenes were observed on the interaction sites or functional groups of the MF molecule. Hence, the adsorption

Table 4
Calculated bond lengths (Å), bond angle (°), charges (Q/e), adsorption energy (E_{ad}/eV), distance (D/Å), HOMO energies (E_{HOMO}/eV), LUMO energies (E_{LUMO}/eV), HOMO-LUMO energy gap (E_g/eV), Fermi level energy (E_F/eV) and dipole moment (D_M/Debye) for the most stable configurations using the B3LYP-D functional.

System	MF-$AlB_{11}N_{12}$	MF-$SiB_{11}N_{12}$	MF-$GeB_{11}N_{12}$	MF-$CB_{11}N_{12}$	MF-$MgB_{11}N_{12}$
R_{X-N}	1.896	1.793	1.903	1.528	2.146
R_{X-N-B}	84.98	86.98	87.98	88.27	96.33
R_{C-NH}	1.324	1.416	1.407	1.417	1.287
D/Å	1.916	1.706	1.803	1.412	2.166
E_{ad}/eV	−2.72	−1.26	−0.93	−0.62	−2.46
Q_X	1.996	−0.985	0.856	0.479	0.602
Q_B	1.074	0.432	0.551	0.493	0.511
Q_N	−1.403	−0.558	−0.537	−0.421	−0.536
Q_{NH2-MF}	−0.880	−0.761	−0.765	−0.758	−0.766
Q_{NH-MF}	−0.980	−0.709	−0.784	−0.607	−0.710
E_{HOMO}	−6.18	−3.73	−3.85	−3.97	−5.46
E_{LUMO}	−1.29	−0.50	−0.55	−0.56	−1.21
E_g/eV	4.89	3.23	3.30	3.41	4.25
ΔE_g (%)	14.79	44.02	45.54	25.05	1.62
E_{FL}	−3.74	−2.12	−2.20	−2.27	−3.34
μ/eV	−3.74	−2.12	−2.20	−2.27	−3.34
η/eV	2.44	1.62	1.65	1.71	2.13
ω/eV	2.85	1.38	1.47	1.50	2.62
S/eV	0.20	0.31	0.30	0.29	0.24
χ/eV	3.74	2.12	2.20	2.27	3.34
D_M	14.297	2.736	2.134	3.397	20.047

energies in models **A** and **B** are considerably greater than in models **C** and **D**.

Infrared spectra (IR) of a MF molecule interacting with $B_{12}N_{12}$ fullerene was studied using the B3LYP functional (Table 7). The N—H stretching mode of a MF molecule interacting with $B_{12}N_{12}$ fullerene takes place in the regions of 3484, 3557, and 3612 cm^{-1}. Bands at 1662, 3513, and 3633 cm^{-1} have been assigned to the NH_2 group of the MF molecule upon the adsorption with $B_{12}N_{12}$ fullerene. The strong adsorption bands at 1597 and 1674 cm^{-1} are probably due to the presence of C—N and N—H stretching vibrations [96]. The absorption bands observed at 3037–3183 cm^{-1} correspond to the C—H group and 1000 cm^{-1} is possibly assigned to the B—NH (MF-$B_{12}N_{12}$) stretching vibration of the adsorbed MF molecule. These vibration frequencies were found to match well with those IR assignments reported for similar studies in the literature [97]. Nurani and co-authors experimentally studied the FT-IR spectrum of metformin and observed that the absorption band at 3160.76 cm^{-1} are due to the N—H stretching vibration of the initial NH_2 group, a band at 1574.59 cm^{-1} corresponds to the N—H bending vibration of the primary NH_2 group and a band at 1062.59 cm^{-1} is due to the presence of the C—N stretching vibration [98], which is close to the calculated results obtained from DFT calculations.

As it is clear in Table 5, the negative values of the E_{ads} for these interactions indicate that these reactions are energetically favorable with a pattern of $GaB_{11}N_{12}$, $AlB_{11}N_{12}$ > $MgB_{11}N_{12}$ > $SiB_{11}N_{12}$ > $GeB_{11}N_{12}$ > $CB_{11}N_{12}$. The formation energies of products of MF interacting with doped-$XB_{11}N_{12}$ fullerenes are also represented in Table 6 and based on the general rule that species having the highest negative formation energy represent more thermodynamically favored behavior, the MF-$GaB_{11}N_{12}$, MF-$AlB_{11}N_{12}$, MF-$MgB_{11}N_{12}$, MF-$SiB_{11}N_{12}$, MF-$GeB_{11}N_{12}$, and MF-$CB_{11}N_{12}$ interactions have enthalpy changes (ΔH_{ads}) of −61.70, −60.47, −55.06, −28.31, −20.64, and −13.24 kcal/mol, respectively. Therefore the formation of a bond between these three mentioned Ga/Al/Mg-$B_{11}N_{12}$ fullerenes are more favorable than those of the Si/C/Ge-$B_{11}N_{12}$ fullerenes. To support these findings, we calculated the Gibbs free energy (ΔG_{ads}) of the studied interaction configurations

Table 5
Calculated bond lengths (R/Å), bond angle (R/°), charges (Q/e), adsorption energy (E_{ad}/eV), distance (D/Å), HOMO energies (E_{HOMO}/eV), LUMO energies (E_{LUMO}/eV), HOMO-LUMO energy gap (E_g/eV), Fermi level energy (E_F/eV) and dipole moment (D_M/Debye) for the most stable configurations using the PW91-D functional.

System	$AlB_{11}N_{12}$	MF-$AlB_{11}N_{12}$	$SiB_{11}N_{12}$	MF-$SiB_{11}N_{12}$	$GeB_{11}N_{12}$	MF-$GeB_{11}N_{12}$	$GaB_{11}N_{12}$	MF-$GaB_{11}N_{12}$
R_{X-N}	1.841	1.894	1.810	1.801	1.923	1.895	1.909	1.944
R_{X-N-B}	82.97	84.74	85.99	85.95	87.05	87.95	84.41	85.90
R_{C-NH}	–	1.330	–	1.419	–	1.415	–	1.324
D/Å	–	1.915	–	1.717	–	1.848	–	1.957
E_{ad}/eV	–	−3.25	–	−1.70	–	−1.61	–	−3.39
Q_X	0.534	0.552	0.680	0.866	0.494	0.661	0.407	0.404
Q_B	0.480	0.407	0.409	0.361	0.505	0.476	0.562	0.491
Q_N	−0.483	−0.550	−0.492	−0.512	−0.487	−0.511	−0.534	−0.553
Q_{NH2-MF}	–	−0.588	–	−0.606	–	−0.624	–	−0.590
Q_{NH-MF}	–	−0.605	–	−0.586	–	−0.589	–	−0.652
E_{HOMO}	−6.47	−5.31	−5.86	−2.90	−6.21	−3.05	−6.48	−5.30
E_{LUMO}	−3.64	−2.11	−1.77	−1.35	−1.80	−1.58	−4.14	−2.04
E_g/eV	2.83	3.20	4.09	1.55	4.41	1.47	2.34	3.26
ΔE_g (%)	–	13.7	–	−62.10	–	−66.67	–	39.32
E_{FL}/eV	−5.06	−3.71	−3.82	−2.13	−4.01	−2.32	−5.31	−3.67
μ/eV	−5.06	−3.71	−3.82	−2.13	−4.01	−2.32	−5.31	−3.67
η/eV	1.42	1.60	2.04	0.78	2.21	0.74	1.17	1.63
ω/eV	9.03	4.30	3.56	2.91	3.64	3.65	12.05	4.13
S/eV	0.35	0.31	0.24	0.65	0.23	0.68	0.43	0.31
χ/eV	5.06	3.71	3.82	2.13	4.01	2.32	5.31	3.67
D_M	3.013	14.41	0.889	3.105	1.436	1.407	2.520	14.26

Table 6
Calculated bond lengths (Å), bond angle (°), charges (Q/e), adsorption energy (E_{ad}/eV), distance (D/Å), HOMO energies (E_{HOMO}/eV), LUMO energies (E_{LUMO}/eV), HOMO-LUMO energy gap (E_g/eV), Fermi level energy (E_F/eV) and dipole moment (D_M/Debye) for the most stable configurations.

System	B3LYP(H_2O)		PW91(H_2O)	
	MF-$B_{12}N_{12}$	MF-$GaB_{11}N_{12}$	MF-$B_{12}N_{12}$	MF-$GaB_{11}N_{12}$
R_{B-N}	1.589	1.476	1.593	1.481
R_{Ga-N}	–	1.954	–	1.989
R_{B-N-Ga}	–	86.96	–	89.77
R_{N-B-N}	100.78	109.67	89.98	110.35
R_{B-N-B}	84.86	–	84.63	–
R_{N-H2}	1.013	1.016	1.022	1.017
R_{N-H}	1.014	1.015	1.021	1.022
R_{C-N}	1.328	1.328	1.335	1.313
D/Å	1.558	1.934	1.555	2.046
E_{ad}/eV	−1.54	−3.12	−1.79	−3.67
Q_B	0.673	0.584	0.570	0.467
Q_{Ga}	–	0.578	–	0.498
Q_N	−0.524	−0.601	−0.460	−0.521
Q_{NH2-MF}	−0.760	−0.755	−0.733	−0.756
Q_{NH-MF}	−0.659	−0.810	−0.617	−0.710
E_{HOMO}	−6.55	−6.45	−5.62	−4.99
E_{LUMO}	−0.54	−0.74	−1.42	−1.52
E_g/eV	6.01	5.71	4.20	3.47
E_{FL}	−3.55	−3.60	−3.52	−3.26
μ/eV	−3.55	−3.60	−3.52	−3.26
η/eV	3.01	2.89	2.10	1.74
ω/eV	2.09	2.26	2.95	3.05
S/eV	0.17	0.18	0.24	0.29
χ/eV	3.55	3.60	3.52	3.26
D_M	15.847	19.645	15.853	30.757

where spontaneity occurrence of a reaction is directly correlated to the negative value of ΔG_{ads} and therefore the more negative value of the ΔG_{ads}, the more thermodynamically favored the reaction. The calculated ΔG_{ads} values in models **A** and **B** were slightly negative with values of −17.22 and −16.85 kcal/mol, respectively. This indicates that these adsorption models are not thermodynamically favorable and stable. The ΔG_{ads} values for the MF-$GaB_{11}N_{12}$, MF-$AlB_{11}N_{12}$, MF-$MgB_{11}N_{12}$, MF-$SiB_{11}N_{12}$, MF-$CB_{11}N_{12}$, and MF-$GeB_{11}N_{12}$ complexes are calculated to be −49.72, −48.39, −44.56, −17.31, −10.08, and −9.31 kcal/mol, respectively. In the case of entropic changes (ΔS_{ads}), it follows a similar trend with the following pattern of the MF-$GaB_{11}N_{12}$ > MF-$AlB_{11}N_{12}$ > MF-$MgB_{11}N_{12}$ > MF-$SiB_{11}N_{12}$ > MF-$CB_{11}N_{12}$ > MF-$GeB_{11}N_{12}$ complexes, showing the highest to the lowest kinetically favored interaction configurations. The lower value of the ΔG_{ads} in comparison with that of the ΔH_{ads} is due to the entropic effect [102].

It has been observed that upon adsorption, the lengths of the C—N, Ge—N, Si—N, Mg—N, Al—N, and Ga—N bonds interacting with the MF molecule somewhat increase (Table 5). Charge analysis indicates that about 0.35, 0.42, and 0.34 |e| of charge were transferred from the MF molecule to the $MgB_{11}N_{12}$, $AlB_{11}N_{12}$, and $GaB_{11}N_{12}$ fullerenes, respectively, which are larger in comparison with the MF molecule interaction with the pure fullerenes. These results reveal that the covalent interactions between the drug molecule and the doping atom (including Mg, Al, and Ga) of $XB_{11}N_{12}$ fullerene were very strong due to the considerable hybridization occurring between the two corresponding orbitals of the adsorbent and the adsorbate species as displayed in Fig. 2. The values of electric dipole moment (DM) of the $CB_{11}N_{12}$, $GeB_{11}N_{12}$, $MgB_{11}N_{12}$, $AlB_{11}N_{12}$, $SiB_{11}N_{12}$ and $GaB_{11}N_{12}$ fullerenes were investigated where the electric dipole moment values are 0.69, 1.55, 0.95, 2.76, 3.24, and 5.41 Debye, respectively (Fig. 3). On the other hand, the DM values for the MF molecule interacting with the $CB_{11}N_{12}$, $GeB_{11}N_{12}$, $SiB_{11}N_{12}$, $AlB_{11}N_{12}$, $GaB_{11}N_{12}$, and $MgB_{11}N_{12}$ fullerenes were calculated to be 3.40, 2.13, 2.73, 14.30, 14.27, and 20.04 Debye, respectively. The presence of polar bonds between the drug molecule and the fullerene (due to the doping of Al, Ga, and Mg atoms) represents significant increases in the dipole moment values due to the strong polarization of the resulting MF-fullerene complexes (see Fig. 3). Due to the adsorption process, the vibrational bands shifted to higher wavelengths as the values of 3381 ($CB_{11}N_{12}$), 3352 ($MgB_{11}N_{12}$), 3359 ($SiB_{11}N_{12}$), 3579 ($GaB_{11}N_{12}$), 3562 ($AlB_{11}N_{12}$), and 3601 cm^{-1} ($GeB_{11}N_{12}$) have been assigned to N—H asymmetric stretching vibrations [103]. As displayed in Table 6, the strong absorption band in the IR spectra at 1656 ($AlB_{11}N_{12}$) and 1661 cm^{-1} ($GaB_{11}N_{12}$) have been assigned to C═N stretching vibrations [104].

For better comprehension of the adsorption processes in these complexes, we studied the electronic properties of the MF molecule adsorbed upon the doped fullerenes via the partial density of states (PDOS) calculations (Fig. 4). Our calculation shows that the drug molecule can significantly affect the electronic properties of the $SiB_{11}N_{12}$ and $GeB_{11}N_{12}$ fullerenes, causing a decrease in the energy band gap for all fullerenes in comparison with other studied fullerenes. In the vicinity of the Fermi energy (E_F), the peaks (new outstanding hybridized peaks) appearing in the MF-$SiB_{11}N_{12}$ and MF-$GeB_{11}N_{12}$ systems are not seen in the PDOS of pure doped fullerenes (data not shown). For these systems, it can be realized that the PDOS proximate for MF-$SiB_{11}N_{12}$ and MF-$GeB_{11}N_{12}$ systems show a new peak in the band gap region thereby lowering the band gap to a large extent as compared to the pure $SiB_{11}N_{12}$ and $GeB_{11}N_{12}$ fullerenes [105]. The results indicate that the energy band gaps (E_g) for the combined systems were reduced from 4.32, 4.26, and 3.76 eV in the pure $MgB_{11}N_{12}$, $AlB_{11}N_{12}$, and $GaB_{11}N_{12}$ fullerenes to 4.25, 4.89, and 4.91 eV after adsorption, respectively. The calculated energies of the Fermi level were −4.67, −5.18, and −5.46 eV for the pure $MgB_{11}N_{12}$, $AlB_{11}N_{12}$, and $GaB_{11}N_{12}$, respectively. Upon the adsorption of the MF molecule, the energies of E_F

Table 7
Thermodynamic parameters of the MF molecule over the pure and doped $XB_{11}N_{12}$ fullerenes using the PW91 method.

Property	ΔH_{ads}	ΔG_{ads}	ΔS_{ads}	υ_{min}	υ_{max}	υ_{N-H}	$\upsilon_{C=N}$
MF	–	–	–	65.61	3639.49	3456.44	1722.27
$B_{12}N_{12}$	–	–	–	326.89	1447.58	–	–
A	−29.54	−17.21	−28.95	13.42	3633.53	3577.13	1674.51
$B_{16}N_{16}$	–	–	–	280.67	1454.23	–	–
B	−28.53	−16.12	−27.56	16.57	3660.88	3538.74	1689.92
$CB_{11}N_{12}$	–	–	–	325.23	1463.32	–	–
MF-$CB_{11}N_{12}$	−13.24	−10.08	−12.65	17.39	3637.46	3381.32	1722.65
$SiB_{11}N_{12}$	–	–	–	273.74	1447.22	–	–
MF-$SiB_{11}N_{12}$	−28.31	−17.31	−27.71	11.44	3634.07	3559.38	1745.68
$AlB_{11}N_{12}$	–	–	–	236.41	1447.31	–	–
MF-$AlB_{11}N_{12}$	−60.47	−48.39	−59.88	23.23	3613.68	3562.42	1656.69
$MgB_{11}N_{12}$	–	–	–	187.51	1451.53	–	–
MF-$MgB_{11}N_{12}$	−55.06	−44.56	−54.47	11.38	3666.50	3552.20	1754/1709
$GeB_{11}N_{12}$	–	–	–	211.28	1447.01	–	–
MF-$GeB_{11}N_{12}$	−20.64	−9.31	−11.32	17.22	3624.16	3601.36	1744.63
$GaB_{11}N_{12}$	–	–	–	188.42	1448.77	–	–
MF-$GaB_{11}N_{12}$	−61.70	−49.72	−61.11	17.84	3617.36	3579.29	1661.71

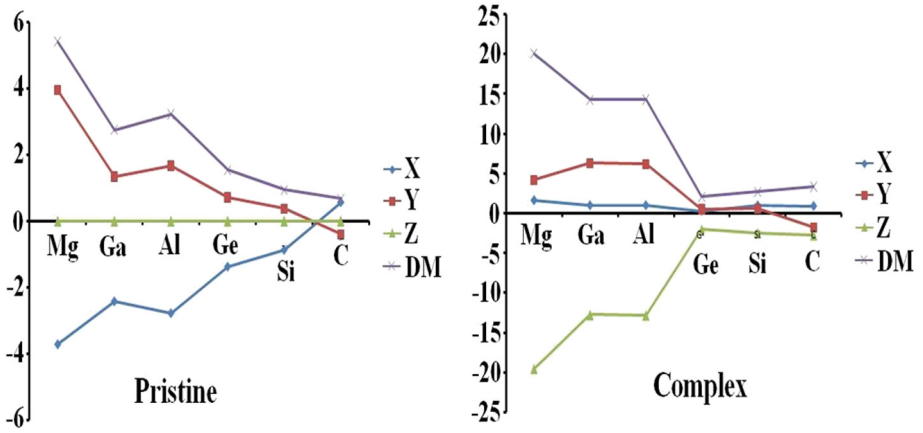

Fig. 3. The values of dipole moment for the MF molecule interacting with the non-metal and metal-doped $B_{12}N_{12}$ fullerenes.

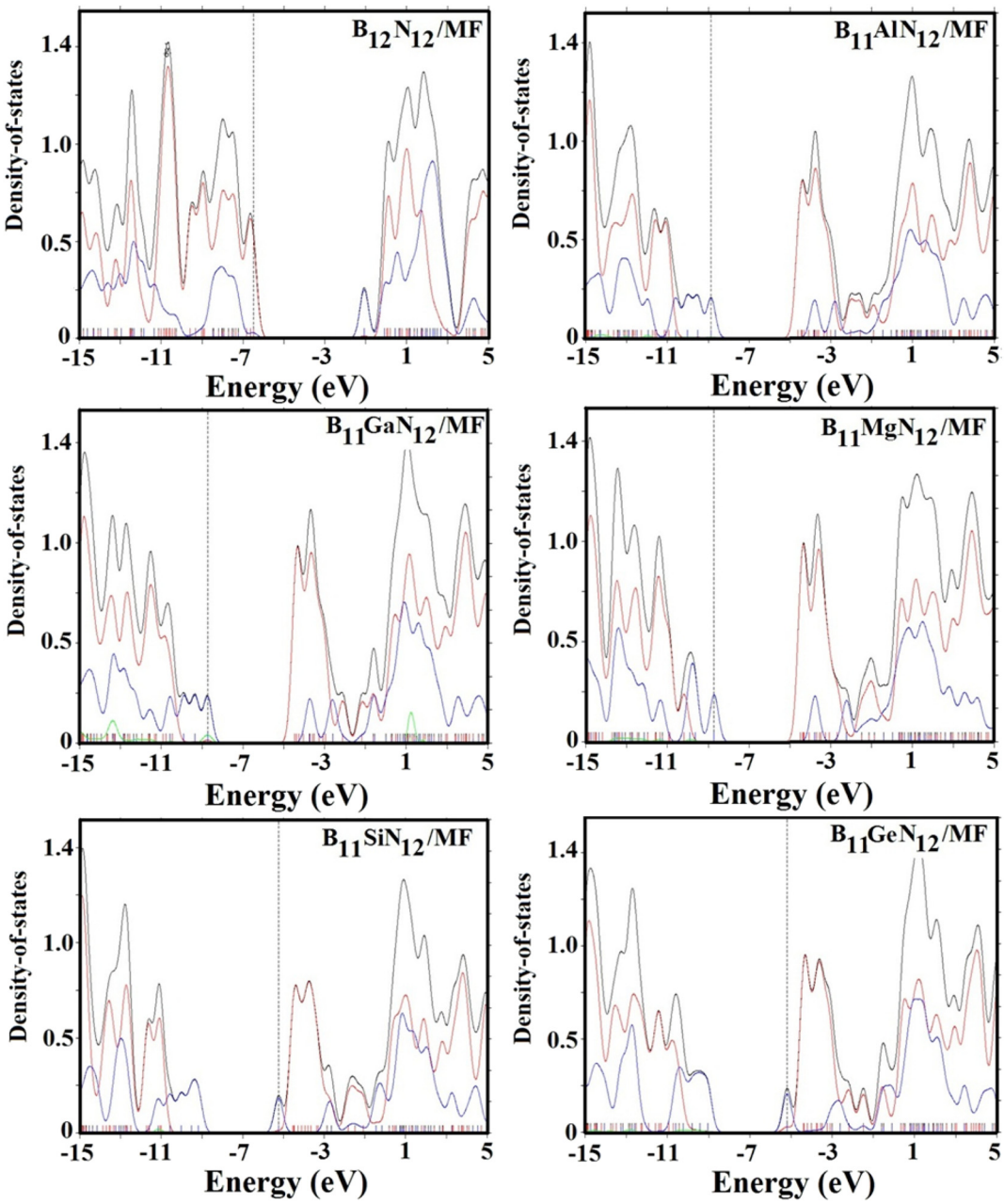

Fig. 4. PDOS spectra for the MF interacting with the pure and doped-$B_{11}N_{12}$ fullerenes.

were increased to −3.33, −3.73, and −3.68 eV, respectively. In addition, the difference in the energies of E_F clearly shows that some meaningful amount of charge has been transferred between the drug molecule and the doping atoms of the $B_{12}N_{12}$ fullerenes.

The highest occupied molecular orbital (HOMO) and lowest unoccupied molecular orbital (LUMO) in the most stable configurations for $AlB_{11}N_{12}$ and $GaB_{11}N_{12}$ fullerenes at the B3LYP level of theory are shown in Figs. 5 and 6 with values in Table 4. The energies of HOMO for the pristine $MgB_{11}N_{12}$, $AlB_{11}N_{12}$, and $GaB_{11}N_{12}$ fullerenes were −6.83, −7.31, and −7.34 eV while the energies of LUMO were −2.51, −3.05, and −3.58 eV, respectively. Table 5 indicates that the HOMO energies for these complexes increased to −5.46, −6.18, and −6.14 eV, while the LUMO energies were about −1.21, −1.29, and −1.23 eV upon the interaction between the MF molecule and the fullerenes ($MgB_{11}N_{12}$, $AlB_{11}N_{12}$, and $GaB_{11}N_{12}$), respectively. Figs. 4 and 5 show the HOMO charge distribution pattern after the interaction and it can be seen that most of the electrons are localized on the surface of the Ga/Al/Mg-$B_{11}N_{12}$ fullerenes while at the same time it is more localized on the surface of the MF drug when it interacts with the Si/Ge/C-$B_{11}N_{12}$ fullerenes. In case of the LUMO charge distribution, more electrons are situated on the MF molecule and the fullerene for the MF-Ga/Al/Mg-$B_{11}N_{12}$ and MF-Si/Ge/C-$B_{11}N_{12}$ interaction systems, respectively. It appears that the nature of the HUMO and LUMO has changed upon adsorption. Moreover, the decrease in the energy band gap followed by the changes in the density of state plots may be attributed to the appearance of the new states associated with the MF molecule in the adsorption systems which are visible in the PDOS plots (Fig. 4). These remarkable differences provide evidence of the important role that these doped atoms ($GeB_{11}N_{12}$ and $SiB_{11}N_{12}$ fullerenes) play in the changes of electronic properties of the $XB_{11}N_{12}$ fullerenes and hence attributes to the sensitivity of this fullerene to MF molecule. One can see that for the $MgB_{11}N_{12}$ fullerene, the new mid-gap states are made inside the E_g which can change the electronic properties due to the change in electron affinity and the ionization potential of the system. As a result, it

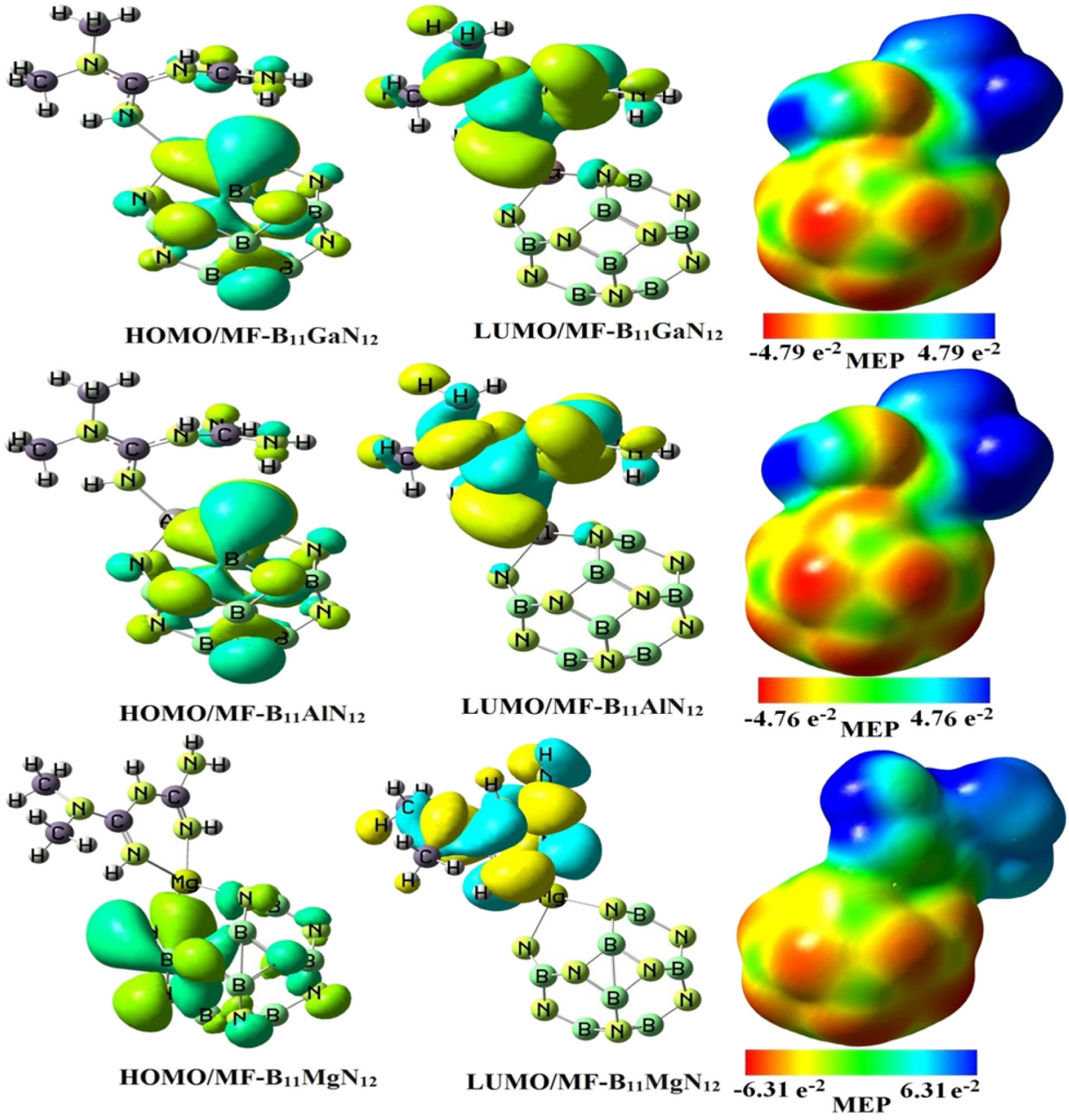

Fig. 5. FMO (HOMO & LUMO) and MEP maps of the MF interacting with doped-$B_{11}N_{12}$ fullerenes elaborated as yellow or red, blue, and light green colors representing electronegative, electropositive, and neutral regions of the structures.

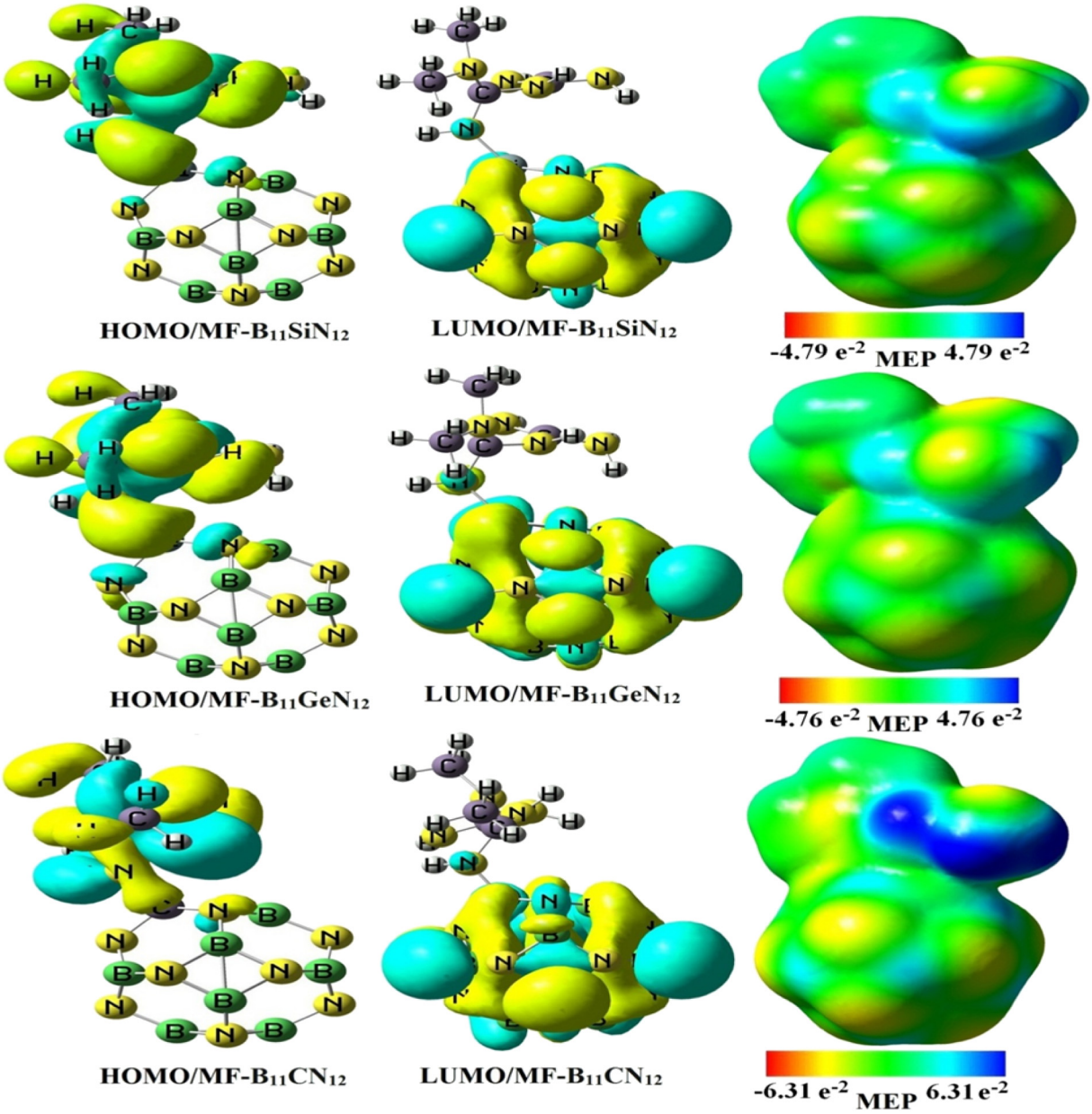

Fig. 6. FMO (HOMO & LUMO) and MEP maps of the MF interacting with doped-$B_{11}N_{12}$ fullerenes elaborated as yellow or red, blue, and light green colors representing electronegative, electropositive, and neutral regions of the structures.

can be seen that the adsorption of the MF drug varies the band edge of the system significantly. Also for the $MgB_{11}N_{12}$ fullerene, it appears that the donor (HOMO) and acceptor (LUMO) energy states are changed upon the adsorption of the MF molecule on the studied fullerenes.

The quantum molecular descriptors of the studied adsorption configurations are also investigated in different situations elaborated are included in the Tables 1–5. The results indicate that global hardness (η) and softness (S) are (3.42 and 0.15 eV) for the pure $B_{12}N_{12}$ and (3.19 and 0.16 eV) for the pure $B_{12}N_{16}$ fullerenes. Upon the interaction of the MF molecule with the $B_{12}N_{12}$ and $B_{16}N_{16}$ fullerenes at all studied configurations, the values of the η decreased while at the same time the values of the S increased. These trends indicate the decrease in the stability of the studied systems and therefore facilitation in the reactivity of the studied substrates as the adsorbent for the MF molecule [106,107]. Table 1 contains values of the electrophilicity index (ω) and electronegativity (x) of (2.69 and 4.29 eV) for the pure $B_{12}N_{12}$ and (2.76 and 4.20 eV) for the pure $B_{12}N_{16}$ fullerenes at B3LYP-D functional and these values are generally increased in case of $XB_{11}N_{12}$ fullerenes where X is Al, Si, Ge, C, Mg and Ga using the same functional as listed in Table 4. Results show that they are reduced upon the adsorption of the MF molecule to the $B_{12}N_{12}$, $B_{16}N_{16}$ and $XB_{11}N_{12}$ fullerene, these values reveal that some charge transfer occurs in the system upon the interaction leading to changes of the electron density of the system upon the interaction. These are more noticeable in the case of the MF molecule adsorption upon the $XB_{11}N_{12}$ fullerenes.

To understand how the MF molecule adsorbed on the pure $B_{12}N_{12}$, $GeB_{11}N_{12}$, $SiB_{11}N_{12}$, $MgB_{11}N_{12}$, $AlB_{11}N_{12}$, and $GaB_{11}N_{12}$ fullerenes influence the electron density, we studied and compared the variance of topology in the electron localization function (ELF) of the most stable states. This should give a good description of the electron space delocalization between the MF molecule and the various fullerenes. The ELF given in Fig. 7 refers to the jellium–like homogeneous electron gas and renormalizes the value between 0.00 and 1.00. The values of 1.0 correspond to the strong localization (red areas), 0.50 equates to free electron gas behavior (green areas) and 0.00 refers to zero localization [108]. Fig. 7 includes ELF space contour plots for the MF molecule

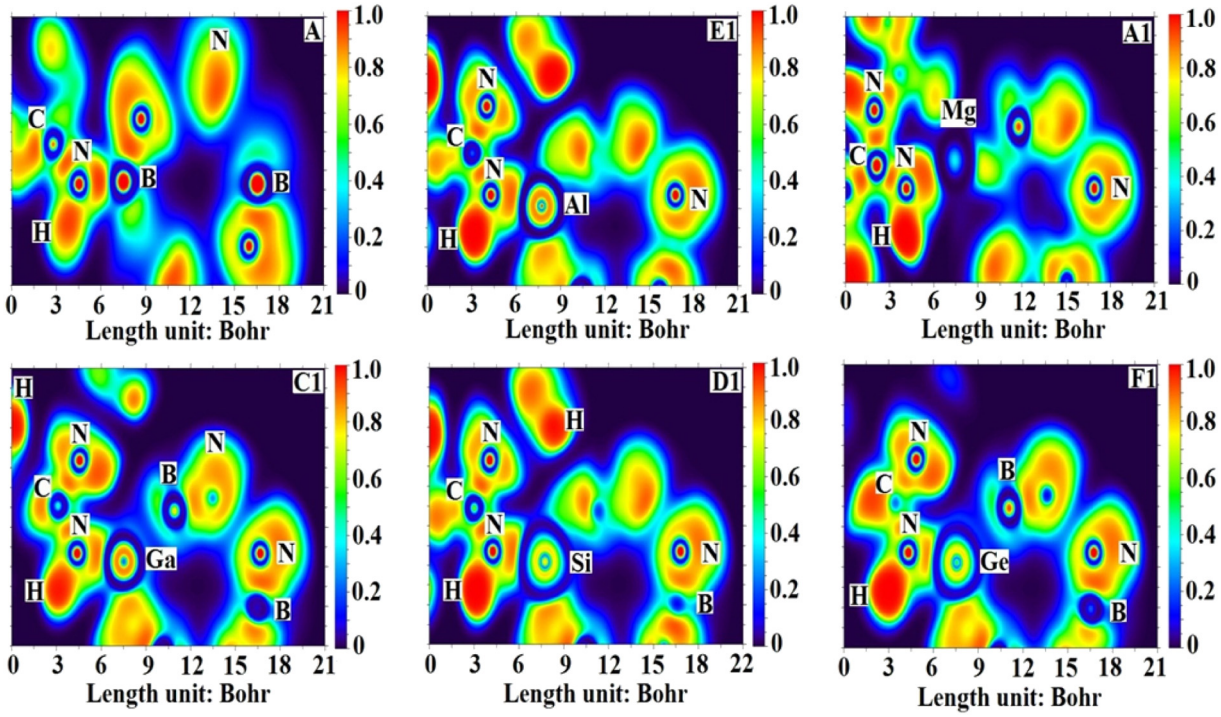

Fig. 7. ELF spectra for the MF interacting with the pure and doped-$B_{11}XN_{12}$ fullerenes.

interacting with the $MgB_{11}N_{12}$, $AlB_{11}N_{12}$ and $GaB_{11}N_{12}$ fullerenes. One can observe a significant localization (red areas) between the nitrogen atom of the drug molecule and the Al, Mg, and Ga atoms of doped-fullerenes that leads to strong covalent interactions in the states A, E1, A1, and C1, respectively. The electrons are completely centralized between the N atom of the drug and the doped-fullerene, where they do share some electrons. As displayed in Fig. 7, the larger ELF value ($Z \approx 1.0$) located on the Al, Ga, and Mg—N bonds exhibits a chemical covalent bond that may be formed through the MF molecule adsorption on the pure and doped fullerenes [109–111]. Also demonstrated in the Fig. 7 are weak chemical interaction between the drug molecule and the doped fullerene in the states D1 and F1 revealing a high sensitivity between them, therefore the release of the MF molecule in such well-known $GeB_{11}N_{12}$ and $SiB_{11}N_{12}$ are easier and could be too fast in contrary to the $MgB_{11}N_{12}$, $AlB_{11}N_{12}$, and $GaB_{11}N_{12}$ fullerenes [79].

4. Conclusions

In summary, the adsorption of the MF molecule on two representative $B_{12}N_{12}$ and $B_{16}N_{16}$ fullerenes has been studied using first-principles calculations. According to binding energy studies, the covalent interaction of MF from its —NH group toward $B_{12}N_{12}$ fullerene is energetically more favorable than $B_{16}N_{16}$ fullerene. The doped atom-$XB_{11}N_{12}$ fullerenes facilitate the adsorption of the MF molecule compared to the pristine $B_{12}N_{12}$ fullerene. The comparison of the theoretical infrared spectra and the experimental Fourier transform infrared spectra was considered to support each other. The results of TDOS plots reveal that the $GeB_{11}N_{12}$ has greater sensitivity to the presence of MF than the $SiB_{11}N_{12}$ while the binding energy and dipole moment studies suggest that the electronic properties of $GaB_{11}N_{12}$ have changed less remarkably than those of $GeB_{11}N_{12}$ and $SiB_{11}N_{12}$ fullerenes. The PW91-D functional gives higher values of adsorption energy and energy gap difference for the same adsorption configuration. The PCM calculations revealed that the selected adsorption configurations are stable in the water medium as a simulation of the body condition. Therefore, we could suggest that the $GeB_{11}N_{12}$ fullerene would be suitable as a biosensor for the detection of metformin drug in environmental systems.

Acknowledgment

The authors would like to acknowledge the Payame Noor University, Tehran, Iran (Research Project Grant No. 2755/2/D96). Mohammad Ramezani Taghartapeh acknowledges Swinburne University of Technology for a SUPRA scholarship. We would like to thank the clinical Research Development Unit (CRDU), Sayad Shirazi Hospital, Golestan University of Medical Sciences, Gorgan, Iran.

References

[1] K. Mahmood, M. Naeem, N.A. Rahimnajjad, Metformin: the hidden chronicles of a magic drug, Eur. J. Intern. Med. 24 (2013) 20–26.
[2] C.V. Rizos, M.S. Elisaf, Metformin and cancer, Eur. J. Pharmacol. 705 (2013) 96–108.
[3] H.-J. Son, J. Lee, S.-Y. Lee, E.-K. Kim, M.-J. Park, K.-W. Kim, S.-H. Park, M.-L. Cho, Metformin attenuates experimental autoimmune arthritis through reciprocal regulation of Th17/Treg balance and osteoclastogenesis, Mediat. Inflamm. 2014 (2014) 1–13.
[4] Q. Weng, B. Wang, X. Wang, N. Hanagata, X. Li, D. Liu, X. Wang, X. Jiang, Y. Bando, D. Golberg, Highly water-soluble, porous, and biocompatible boron nitrides for anticancer drug delivery, ACS Nano 8 (6) (2014) 6123–6130.
[5] P. Balasubramanian, T. Büttner, V. Miguez Pacheco, A.R. Boccaccini, Boron-containing bioactive glasses in bone and soft tissue engineering, J. Eur. Ceram. Soc. 38 (2018) 855–869.
[6] X. Chen, P. Wu, M. Rousseas, D. Okawa, Z. Gartner, A. Zettl, C.R. Bertozzi, Boron nitride nanotubes are noncytotoxic and can be functionalized for interaction with proteins and cells, J. Am. Chem. Soc. 131 (2009) 890–891.
[7] G. Ciofani, V. Raffa, A. Menciassi, A. Cuschieri, Cytocompatibility, interactions, and uptake of polyethyleneimine-coated boron nitride nanotubes by living cells: confirmation of their potential for biomedical applications, Biotechnol. Bioeng. 101 (2008) 850–858.
[8] P. Umapathi, J. Ayyappan, S.D. Quine, Quantitative determination of metformin hydrochloride in tablet formulation containing croscarmellose sodium as disintegrant by HPLC and UV spectrophotometry, Trop. J. Pharm. Res. 11 (2012) 107–116.
[9] M.A.S. Marques, A. de S. Soares, O.W. Pinto, P.T.W. Barroso, D.P. Pinto, M.F. Filho, E.W. Barroso, Simple and rapid method determination for metformin in human plasma using high performance liquid chromatography tandem mass spectrometry: application to pharmacokinetic studies, J. Chromatogr. B 852 (2007) 308–316.

[10] C. Georgita, I. Sora, F.L. Albu, C.M. Monciu, Comparison of a LC/MS method with a LC/UV method for the determination of metformin in plasma samples, Farmacia 58 (2010) 158–169.
[11] S.R. Dhaneshwar, J.V. Salunkhe, V.K. Bhusari, Validated HPTLC method for simultaneous estimation of metformin hydrochloride, atorvastatin, and glimepiride in bulk drug and formulation, J. Anal. Bioanal. Tech. 1 (2010) 1–5.
[12] R.Q. Gabr, R.S. Padwal, D.R. Brocks, Determination of metformin in human plasma and urine by high-performance liquid chromatography using small sample volume and conventional octadecylsilane column, J. Pharmacol. Pharm. Sci. 13 (2010) 486–494.
[13] B.G. Charles, N.W. Jacobsen, P.J. Ravenscroft, Rapid liquid-chromatographic determination of metformin in plasma and urine, Clin. Chem. 27 (1981) 434–436.
[14] B. Chiavarino, M.E. Crestoni, A.D. Marzio, S. Fornarini, Determination of sulfonamide antibiotics by gas chromatography coupled with atomic emission detection, J. Chromatogr. B 706 (1998) 269–277.
[15] M.S. Lennard, C. Casey, G.T. Tucker, H.F. Woods, Determination of metformin in biological samples, Br. J. Clin. Pharmacol. 6 (1978) 183–185.
[16] J.M. Calatayud, P.C. Falco, M.C.P. Marti, Metformin and moroxidine determination with Cu(II), Anal. Lett. 18 (1985) 1381–1390.
[17] N. Sattarahmady, H. Heli, F. Faramarzi, Nickel oxide nanotubes–carbon microparticles/Nafion nanocomposite for the electro-oxidation and sensitive detection of metformin, Talanta 82 (2010) 1126–1135.
[18] X.J. Tian, J.F. Song, X.-J. Luan, Y. Wang, Q. Shi, Determination of metformin based on amplification of its voltammetric response by a combination of molecular wire and carbon nanotubes, Anal. Bioanal. Chem. 386 (2006) 2081–2086.
[19] X.J. Tian, J.F. Song, Catalytic action of copper (II) ion on electrochemical oxidation of metformin and voltammetric determination of metformin in pharmaceuticals, J. Pharm. Biomed. Anal. 44 (2007) 1192–1196.
[20] S. Skrzypek, V. Mirceski, W. Ciesielski, A. Sokołowski, R. Zakrzewski, Direct determination of metformin in urine by adsorptive catalytic square-wave voltammetry, J. Pharm. Biomed. Anal. 45 (2007) 275–281.
[21] L. Yongming, L. Guizhi, Voltammetric behavior of metformin hydrochloride on glassy carbon electrode and its application, Chin. J. Anal. Chem. 29 (2001) 2001–2009.
[22] J.Z. Song, H.F. Chen, S.J. Tian, Z.P. Sun, Determination of metformin in plasma by capillary electrophoresis using field-amplified sample stacking technique, J. Chromatogr. B 708 (1998) 277–283.
[23] M.S. Refat, Synthesis and characterization of norfloxacin–transition metal complexes (group 11, IB): spectroscopic, thermal, kinetic measurements and biological activity, Spectrochim. Acta A 68 (2007) 1393–1405.
[24] M.R. Sohrabi, N. Kamali, M. Khakpour, Simultaneous spectrophotometric determination of metformin hydrochloride and glibenclamide in binary mixtures using combined discrete and continuous wavelet transforms, Anal. Sci. 27 (2011) 1037–1041.
[25] G. Mubeen, K. Noor, M.N. Vimala, Spectrophotometric method for estimation of metformin hydrochloride, Int. J. Chem. Technol. Res. 2 (2010) 1186–1187.
[26] S. Ashour, R. Kabbani, Direct spectrophotometric determination of metformin hydrochloride in pure form and in drug formulations, Anal. Lett. 36 (2003) 361–370.
[27] M.S. Arayne, N. Sultana, M.H. Zuberi, F.A. Siddiqui, Spectrophotometric quantitation of metformin in bulk drug and pharmaceutical formulations using multivariate technique, Indian J. Pharm. Sci. 71 (2009) 331–335.
[28] G. Mubeen, K. Noor, Spectrophotometric method for analysis of metformin hydrochloride, Indian J. Pharm. Sci. 71 (2009) 100–102.
[29] M.G. El-Bardicy, S.Z. El-Khateeb, A.S. Ahmad, H.N. Assaad, Spectrophotometric determination of metformin via charge–transfer complex with iodine, Spectrosc. Lett. 22 (1989) 1173–1181.
[30] P.S. Sudarshan, C.G. Bonde, Development and validation of analytical method for simultaneous estimation of glibenclamide and metformin-HCl in bulk and tablets using UV–visible spectroscopy, Int. J. Chem. Technol. Res. 1 (2009) 905–909.
[31] S.M. Riad, M.R. Rezk, G.Y. Mahmoud, A.E. Abdel Aleem, Spectrophotometric determination of sitagliptin and metformin in their pharmaceutical formulation, Int. J. Compr. Pharm. 3 (2012) 1–4.
[32] I.H.I. Habib, M.S. Kamel, Near infra-red reflectance spectroscopic determination of metformin in tablets, Talanta 60 (2003) 185–190.
[33] H.H. Gadape, K.S. Perikh, Quantitative determination and validation of metformin hydrochloride in pharmaceutical using quantitative nuclear magnetic resonance spectroscopy, J. Chem. 8 (2011) 767–781.
[34] F. Bentefrit, G. Morgant, B. Viossat, S. Leonce, N. Guilbaud, A. Pierre, G. Atassi, N.H. Dung, Synthesis and antitumor activity of the metformin platinum(IV) complex: crystal structure of the tetrachloro(metformin)platinum(IV) dimethylsulfoxide solvate, J. Inorg. Biochem. 68 (1997) 53–59.
[35] B. Viossat, A. Tomas, N.-H. Dung, L'hydrogenocarbonate de Bis(*N*,*N*-dimethylbiguanide) Cuivre(II), $[Cu(C_4H_{11}N_5)2]2HCO_3$, Acta Crystallogr. 51 (1995) 213–215.
[36] N.K. Rao, M.M. Annapurna, Copper and nickel complexes of metformin: synthesis, characterization, and pharmacodynamic evaluation, JASA 3 (2007) 43–46.
[37] S.M. Abu-el-Wafa, M.A. El-Ries, F.H. Ahmed, Formation of metformin complexes with some transition metal ions: their biological activity, Inorg. Chim. Acta 136 (1987) 127–131.
[38] S. S. Sharma, J. V. Ramani, D. P. Dalwadi, J. J. Bhalodia, N. K. Patel, D. D. Patel, R. K. Patel, New ternary transition metal complexes of 2-{[(2-aminophenyl) imino] methyl}phenol and metformin: synthesis, characterization, and antimicrobial activity, E-J. Chem. 8 (2011) 361–367.
[39] A. Moghimi, H.R. Khavassi, F. Dashtestani, D. Kordestani, A. Ekram Jafari, B. Maddah, S.M. Moosavi, A ternary tetracoordinated Pd(II) complex with metformin and dipicolinate: synthesis, characterization, and crystal structure, J. Mol. Struct. 996 (2011) 38–41.
[40] H. Zhao, X. Yuan, J. Yu, Y. Huang, C. Shao, F. Xiao, L. Lin, Y. Li, L. Tian, Magnesium stabilized multifunctional DNA nanoparticles for tumor-targeted and pH-responsive drug delivery, ACS Appl. Mater. Interfaces 10 (18) (2018) 15418–15427.
[41] L. Cai, J. Chen, Z. Liu, H. Wang, H. Yang, W. Ding, Magnesium oxide nanoparticles: effective agricultural antibacterial agent against *Ralstonia solanacearum*, Front. Microbiol. 9 (2018) 1–19.
[42] A. Suryavanshi, K. Khanna, K.R. Sindhu, J. Bellare, R. Srivastava, Magnesium oxide nanoparticle-loaded polycaprolactone composite electrospun fiber scaffolds for bone–soft tissue engineering applications: in-vitro and in-vivo evaluation, Biomed. Mater. 12 (2017), 055011. .
[43] T. Oku, A. Nishiwaki, I. Narita, Formation and atomic structures of B_nN_n (n = 24–60) clusters studied by mass spectrometry, high-resolution electron microscopy and molecular orbital calculations, Physica B 351 (2004) 184–190.
[44] T. Oku, A. Nishiwaki, I. Narita, Formation and structure of $B_{28}N_{28}$ clusters studied by mass spectrometry and molecular orbital calculation, Solid State Commun. 130 (2004) 171–173.
[45] T. Oku, A. Nishiwaki, I. Narita, Formation and structures of $B_{36}N_{36}$ and $Y@B_{36}N_{36}$ clusters studied by high-resolution electron microscopy and mass spectrometry, J. Phys. Chem. Solids 65 (2004) 369–372.
[46] R. Li, L.-H. Gan, Q. Li, J. An, Structure and stability of $B_{13}N_{13}$ polyhedrons with octagon(s), Chem. Phys. Lett. 482 (2009) 121–124.
[47] W.H. Moon, M.S. Son, H.J. Hwang, Theoretical study on structure of boron nitride fullerenes, Appl. Surf. Sci. 253 (2007) 7078–7081.
[48] Y.-Z. Lan, W.-D. Cheng, D.-S. Wu, X.-D. Li, H. Zhang, Y.-J. Gong, J. Shen, F.-F. Li, Theoretical studies of third-order nonlinear optical response for $B_{12}N_{12}$, $B_{24}N_{24}$ and $B_{36}N_{36}$ clusters, J. Mol. Struct. THEOCHEM 730 (2005) 9–15.
[49] X.F. Fan, Z. Zhu, Z.X. Shen, J.-L. Kuo, On the use of bond-counting rules in predicting the stability of $C_{12}B_6N_6$ fullerene, J. Phys. Chem. C 112 (2008) 15691–15696.
[50] M.D. Esrafili, P. Nematollahi, R. Nurazar, A comparative study of CO oxidation reaction over pristine and C-doped boron nitride fullerene, RSC Adv. 6 (2016) 17172–17178.
[51] M.T. Baei, A.S. Ghasemi, E. Tazikeh Lemeski, A. Soltani, N. Gholami, BN nanotube serving as a gas chemical sensor for N_2O by parallel electric field, J. Clust. Sci. 27 (2016) 1081–1096.
[52] M.T. Baei, $B_{12}N_{12}$ sodalite like cage as potential sensor for hydrogen cyanide, Comput. Theor. Chem. 1024 (2013) 28–33.
[53] T. Oku, A. Nishiwaki, I. Narita, Formation and atomic structure of $B_{12}N_{12}$ nanocage clusters studied by mass spectrometry and cluster calculation, Sci. Technol. Adv. Mater. 5 (2004) 635–638.
[54] T. Oku, T. Hirano, M. Kuno, T. Kusunose, K. Niihara, K. Suganuma, Synthesis, atomic structures and properties of carbon and boron nitride fullerene materials, Mater. Sci. Eng. B 74 (2000) 206–217.
[55] T. Oku, M. Kuno, H. Kitahara, I. Narita, Formation, atomic structures and properties of boron nitride and carbon nanocage fullerene materials, Int. J. Inorg. Mater. 3 (2001) 597–612.
[56] A. Soltani, M.T. Baei, E. Tazikeh Lemeski, M. Shahini, Sensitivity of BN nano-cages to caffeine and nicotine molecules, Superlattice. Microst. 76 (2014) 315–325.
[57] S. Yourdkhani, T. Korona, N.L. Hadipour, Structure and energetics of complexes of $B_{12}N_{12}$ with hydrogen halides-SAPT (DFT) and MP2 study, J. Phys. Chem. A 119 (24) (2015) 6446–6467.
[58] A. Soltani, M.T. Baei, M. Ramezani Taghartapeh, E. Tazikeh Lemeski, S. Shojaee, Phenol interaction with different nano-cages with and without an electric field: a DFT study, Struct. Chem. 26 (2015) 685–693.
[59] A. Soltani, M.T. Baei, M. Mirarab, M. Sheikhi, E. Tazikeh Lemeski, The electronic and structural properties of BN and BP nano-cages interacting with OCN^-: a DFT study, J. Phys. Chem. Solids 75 (2014) 1099–1105.
[60] J. Hosseini, A. Rastgoub, R. Moradi, F-encapsulated $B_{12}N_{12}$ fullerene as an anode for Li-ion batteries: a theoretical study, J. Mol. Liq. 225 (2017) 913–918.
[61] X.-Y. Cui, J.-F. Jia, B.-S. Yang, P. Yang, H.-S. Wu, Ab initio investigation of hydrogenation of endohedral $X@(BN)_{16}$ complexes (X = Li^+, Na^+, K^+, Mg^{2+}, Ne, O^{2-}, S^{2-}, F^-, Cl^-), J. Mol. Struct. THEOCHEM 953 (2010) 1–6.
[62] M.T. Baei, M. Ramezani Taghartapeh, E. Tazikeh Lemeski, A. Soltani, A computational study of adenine, uracil, and cytosine adsorption upon AlN and BN nanocages, Physica B 444 (2014) 6–13.
[63] M.D. Esrafili, R. Nurazar, Methylamine adsorption and decomposition on $B_{12}N_{12}$ nanocage: a density functional theory study, Surf. Sci. 626 (2014) 44–48.
[64] N. Injan, J. Sirijaraensreb, J. Limtrakul, Decomposition of nitrous oxide on Fe-doped boron nitride nanotubes: the ligand effect, Phys. Chem. Chem. Phys. 16 (2014) 23182–23187.
[65] M. Bezi Javan, A. Soltani, A.S. Ghasemi, E. Tazikeh Lemeski, N. Gholamic, H. Balakheyli, Ga-doped and antisite double defects enhance the sensitivity of boron nitride nanotubes towards soman and chlorosoman, Appl. Surf. Sci. 411 (2017) 1–10.
[66] A. Soltani, S. Ghafouri Raz, V. Joveini Rezaei, A. Dehno Khalaji, M. Savar, Ab initio investigation of Al- and Ga-doped single-walled boron nitride nanotubes as ammonia sensor, Appl. Surf. Sci. 263 (2012) 619–625.
[67] A. Bahrami, S. Seidi, T. Baheri, M. Aghamohammadi, A first-principles study on the adsorption behavior of amphetamine on pristine, P- and Al-doped $B_{12}N_{12}$ nanocages, Superlattice. Microst. 64 (2013) 265–273.
[68] E.C. Anota, G.H. Cocoletzi, GGA-based analysis of the metformin adsorption on BN nanotubes, Phys. E. 56 (2014) 134–140.
[69] M. Bezi Javan, A. Soltani, Z. Azmoodeh, N. Abdolahi, N. Gholami, A DFT study on the interaction between 5-fluorouracil and $B_{12}N_{12}$ nanocluster, RSC Adv. 6 (2016) 104513–104521.
[70] A. Soltani, A. Sousaraei, M. Bezi Javan, M. Eskandaric, H. Balakheyli, Electronic and optical properties of 5-AVA functionalized BN nanoclusters: a DFT study, New J. Chem. 40 (2016) 7018.

[71] M.J. Frisch, G.W. Trucks, H.B. Schlegel, G.E. Scuseria, M.A. Robb, J.R. Cheeseman, J.A. Montgomery Jr., T. Vreven, K.N. Kudin, J.C. Burant, J.M. Millam, S.S. Iyengar, J. Tomasi, V. Barone, B. Mennucci, M. Cossi, G. Scalmani, N. Rega, G.A. Petersson, H. Nakatsuji, M. Hada, M. Ehara, K. Toyota, R. Fukuda, J. Hasegawa, M. Ishida, T. Nakajima, Y. Honda, O. Kitao, H. Nakai, M. Klene, X. Li, J.E. Knox, H.P. Hratchian, J.B. Cross, V. Bakken, C. Adamo, J. Jaramillo, R. Gomperts, R.E. Stratmann, O. Yazyev, A.J. Austin, R. Cammi, C. Pomelli, J.W. Ochterski, P.Y. Ayala, K. Morokuma, G.A. Voth, P. Salvador, J.J. Dannenberg, V.G. Zakrzewski, S. Dapprich, A.D. Daniels, M.C. Strain, O. Farkas, D.K. Malick, A.D. Rabuck, K. Raghavachari, J.B. Foresman, J.V. Ortiz, Q. Cui, A.G. Baboul, S. Clifford, J. Cioslowski, B.B. Stefanov, G. Liu, A. Liashenko, P. Piskorz, I. Komaromi, R.L. Martin, D.J. Fox, T. Keith, M.A. AlLaham, C.Y. Peng, A. Nanayakkara, M. Challacombe, P.M.W. Gill, B. Johnson, W. Chen, M.W. Wong, C. Gonzalez, J.A. Pople, Gaussian 09, Revision A01, Gaussian, Inc., Wallingford, CT, 2009.
[72] S. Tsuzuki, H.P. Luthi, Interaction energies of van der Waals and hydrogen bonded systems calculated using density functional theory: assessing the PW91 model, J. Chem. Phys. 114 (2001) 3949–3957.
[73] S. Grimme, Semiempirical GGA-type density functional constructed with a long-range dispersion correction, J. Comput. Chem. 27 (2006) 1787–1799.
[74] A.D. Becke, Density-functional thermochemistry. III. The role of exact exchange, J. Chem. Phys. 98 (1993) 5648–5652.
[75] C. Lee, W. Yang, R.G. Parr, Development of the Colle-Salvetti correlation-energy formula into a functional of the electron density, Phys. Rev. B 37 (1988) 785–789.
[76] B. Civalleri, L. Maschio, P. Ugliengo, C.M. Zicovich-Wilson, Role of dispersive interactions in the CO adsorption on MgO (001): periodic B3LYP calculations augmented with an empirical dispersion term, Phys. Chem. Chem. Phys. 12 (2010) 6382–6386.
[77] F. Zhao, Y. Wang, M. Zhu, L. Kang, C-doped boron nitride fullerene as a novel catalyst for acetylene hydrochlorination: a DFT study, RSC Adv. 5 (2015) 56348–56355.
[78] J. Lan, D. Cao, W. Wang, B. Smit, Doping of alkali, alkaline-earth, and transition metals in covalent-organic frameworks for enhancing CO_2 capture by first-principles calculations and molecular simulations, ACS Nano (7) (2010) 4225–4237.
[79] E. Duverger, T. Gharbi, E. Delabrousseb, F. Picaud, Quantum study of boron nitride nanotubes functionalized with anticancer molecules, Phys. Chem. Chem. Phys. 16 (2014) 18425–18432.
[80] E. Shakerzadeh, E. Khodayar, S. Noorizadeh, Theoretical assessment of phosgene adsorption behavior onto pristine, Al- and Ga-doped $B_{12}N_{12}$ and $B_{16}N_{16}$ nanoclusters, Comput. Mater. Sci. 118 (2016) 155–171.
[81] A. Soltani, M. Bezi Javan, Carbon monoxide interactions with pure and doped $B_{11}XN_{12}$ (X = Mg, Ge, Ga) nano-clusters: a theoretical study, RSC Adv. 5 (2015) 90621–90631.
[82] T. Oku, A. Nishiwaki, I. Narita, Formation and atomic structure of $B_{12}N_{12}$ nanocage clusters studied by mass spectrometry and cluster calculation, Sci. Technol. Adv. Mater. 5 (2004) 635–645.
[83] M.S. Hoseininezhad-Namin, P. Pargolghasemi, S. Alimohammadi, A. Shokuhi Rad, L. Taqavi, Quantum chemical study on the adsorption of metformin drug on the surface of pristine, Si- and Al-doped (5, 5) SWCNTs, Phys. E. 90 (2017) 204–213.
[84] V. Renganayaki, S. Srinivasan, HF, DFT computations and spectroscopic study of the vibrational and thermodynamic properties of metformin, Int. J. PharmTech Res. 3 (2011) 1350–1358.
[85] N.-A. Rangel-Vázquez, N.L. Delgadillo-Amendariz, C.L. Salas-Aguilar, Analysis of metformin applied different tools, computationals for determine all the characteristics of drug, J. Nanomed. Res. 2 (2015), 00023.
[86] G-h. Fan, S. Zhu, X-k. Li, K. Ni, H. Xu, Ab initio investigation of pristine and doped single-walled boron nitride nanotubes as acetone sensor, Comput. Theor. Chem. 1115 (2017) 208–216.
[87] A.A. Darwisha, M.M. Fadlallah, A. Badawi, A.A. Maarouf, Adsorption of sugars on Al- and Ga-doped boron nitride surfaces: a computational study, Appl. Surf. Sci. 377 (2016) 9–16.
[88] A. Shokuhi Rad, D. Zareyee, M. Peyravi, M. Jahanshahi, Surface study of gallium- and aluminum-doped graphenes upon adsorption of cytosine: DFT calculations, Appl. Surf. Sci. 401 (2017) 156–171.
[89] A. Shokuhi Rad, Study of dimethyl ester interaction on the surface of Ga-doped graphene: application of density functional theory, J. Mol. Liq. 229 (2017) 1–5.
[90] P.A. Denis, Band gap opening of monolayer and bilayer graphene doped with aluminium, silicon, phosphorus, and sulfur, Chem. Phys. Lett. 492 (2010) 251–257.
[91] X.-Y. Liang, N. Ding, S.-P. Ng, C.-M. Lawrence Wu, Adsorption of gas molecules on Ga-doped graphene and effect of applied electric field: a DFT study, Appl. Surf. Sci. 411 (2017) 11–17.
[92] A. Ahmadi Peyghan, A. Soltani, A.A. Pahlevani, Y. Kanani, So. Khajeh, A first-principles study of the adsorption behavior of CO on Al- and Ga-doped single-walled BN nanotubes, Appl. Surf. Sci. 270 (2013) 25–32.
[93] A. Soltani, M.T. Baei, E. Tazikeh Lemeski, A.A. Pahlevani, The study of SCN-adsorption on B12N12 and B16N16 nano-cages, Superlattice. Microst. 75 (2014) 716–724.
[94] N. Saikia, R.C. Deka, Theoretical study on pyrazinamide adsorption onto covalently functionalized (5, 5) metallic single-walled carbon nanotube, Chem. Phys. Lett. 500 (2010) 65–70.
[95] D. Farmanzadeh, H. Rezainejad, Adsorption of diazinon and hinosan molecules on the iron-doped boron nitride nanotubes surface in gas phase and aqueous solution; a computational study, Appl. Surf. Sci. 364 (2016) 862–869.
[96] G. Socrates, Infrared Characteristic Group Frequencies, 1st ed. John Wiley, New York, 1980.
[97] R. Shanmugam, D.N. Sathyanarayana, Raman and polarized infrared spectra of pyridine-2-thione, Spectrochim. Acta A 40 (1984) 757–761.
[98] M. Nurani, V. Akbari, A. Taheri, Preparation and characterization of metformin surface modified cellulose nanofiber gel and evaluation of its anti-metastatic potentials, Carbohydr. Polym. 165 (2017) 322–333.
[99] A. Shokuhi Rad, K. Ayub, O_3 and SO_2 sensing concept on extended surface of $B_{12}N_{12}$ nanocages modified by nickel decoration: a comprehensive DFT study, Solid State Sci. 69 (2017) 22–30.
[100] M.S. Refat, F.M. Al-Azab, H.M.A. Al-Maydama, R.R. Amin, Y.M.S. Jamil, M.I. Kobeasy, Spectrochim. Acta A 142 (2015) 392–404.
[101] A. Soltani, M.T. Baei, E. Tazikeh Lemeski, S. Kaveh, H. Balakheyli, A DFT study of 5-fluorouracil adsorption on the pure and doped BN nanotubes, J. Phys. Chem. Solids 86 (2015) 57–64.
[102] M.T. Baei, E. Tazikeh Lemeski, A. Soltani, DFT study of the adsorption of H_2O_2 inside and outside $Al_{12}N_{12}$ nano-cage, Russ. J. Phys. Chem. A 91 (2017) 1528–1535.
[103] G. Socrates, Infrared Characteristic Group Frequencies, 1st ed. Wiley, New York, 1980.
[104] L.J. Bellamy, The Infrared Spectra of Complex Molecules, 3rd ed. Chapman and Hall, London, 1975.
[105] S. Saha, P. Sarkar, Understanding the interaction of DNA–RNA nucleobases with different ZnO nanomaterials, Phys. Chem. Chem. Phys. 16 (2014) 15355–15366.
[106] N. Saikia, R.C. Deka, Density functional study on noncovalent functionalization of pyrazinamide chemotherapeutic with graphene and its prototypes, New J. Chem. 38 (2014) 1116–1128.
[107] A. Shokuhi Rad, K. Ayub, Ni adsorption on Al12P12 nano-cage: a DFT study, J. Alloys Compd. 678 (2016) 317–324.
[108] A.D. Becke, K.E. Edgecombe, A simple measure of electron localization in atomic and molecular systems, J. Chem. Phys. 92 (1990) 5397–5403.
[109] A. Soltani, M. Bezi Javan, M.S. Hoseininezhad-Namin, N. Tajabor, E. Tazikeh Lemeski, F. Pourarian, Interaction of hydrogen with Pd- and Co-decorated C_{24} fullerenes: density functional theory study, Synth. Met. 234 (2017) 1–8.
[110] A. Soltani, M. Bezi Javan, M.T. Baei, Z. Azmoodeh, Adsorption of chemical warfare agents over C_{24} fullerene: effects of decoration of cobalt, J. Alloys Compd. 735 (2018) 2148–2161.
[111] A. Soltani, M. Ramezani Taghartapeh, M. Bezi Javan, P.J. Mahon, Z. Azmoodeh, E. Tazikeh Lemeski, I.V. Kityk, Theoretical studies of hydrazine detection by pure and Al defected MgO nanotubes, Phys. E. 97 (2018) 239–249.